Oral antigen exposure under co-stimulation blockade generates Treg cells to establish immune tolerance despite prior sensitization

Masaya Arai[1]*, Ryoji Kawakami[1,2]*, Yamami Nakamura[1], Yoko Naito[3], Daisuke Motooka[3], Atsushi Sugimoto[1], Tomiko Kimoto[1], Naganari Ohkura[1,4], Norihisa Mikami[1], and Shimon Sakaguchi[1,2]†

[1] Department of Experimental Immunology, Immunology Frontier Research Center, Osaka University, 3-1, Yamadaoka, 565-0871, Suita, Osaka, Japan
[2] Department of Experimental Immunology, Institute for Life and Medical Sciences, Kyoto University, Sakyo-ku, 606-8507 Kyoto, Japan
[3] Genome Information Research Center, Research Institute for Microbial Diseases, Osaka University, 3-1, Yamadaoka, 565-0871, Suita, Osaka, Japan
[4] Department of Frontier Research in Tumor Immunology, Graduate School of Medicine, Osaka University, 3-1, Yamadaoka, 565-0871, Suita, Osaka, Japan
* These authors contributed equally to this work
† Corresponding author. Email: shimon@ifrec.osaka-u.ac.jp (S.S.)

Abstract
Antigen-specific oral tolerance is effective in preventing harmful immune responses in antigen-non-sensitized animals but difficult to induce in those already antigen-primed. Here, we show in mice that feeding of antigen-containing diet generates in mesenteric lymph nodes and intestinal lamina propria peripherally derived regulatory T (pTreg) cells that exhibit a terminally differentiated effector phenotype as seen with tissue-resident thymus-derived Treg (tTreg) cells. Antigen feeding also enables the generated pTreg cells to acquire Treg-specific epigenomic changes in Treg signature genes including *Foxp3*, hence the stability of Treg-specific function. Cessation of antigen feeding, however, results in decline in oral tolerance with diminution of pTreg cells. Transcriptomic comparison with tTreg cells has revealed that pTreg cells induced by antigen feeding predominantly express CD101. $CD101^+$ Treg cells with a similar phenotype and epigenetic alterations can be generated *in vitro* from antigen-primed naïve $CD4^+$ T cells by blockade of CD28-mediated co-stimulation during TGF-β-dependent Treg induction. Furthermore, *in vivo* CD28 signal blockade by CTLA-4-immunoglobulin fusion protein (CTLA4-Ig) before antigen feeding can establish oral tolerance in the mice precedingly antigen-sensitized by a non-oral route. The CTLA4-Ig treatment not only suppresses activation of antigen-reactive conventional T cells but also facilitates their differentiation into antigen-specific $CD101^+$ pTreg cells. Thus, continuous oral antigen administration combined with CD28 co-stimulation blockade generates a specific type of antigen-specific functionally stable pTreg cells, which can establish long-term systemic antigen-specific immune tolerance even in antigen-pre-sensitized animals. This strategy for mucosal tolerance induction would be instrumental in treating chronic allergy and other immunological diseases in humans.

Introduction

Oral tolerance is antigen-specific systemic immunological unresponsiveness induced by intestinal exposure to antigens derived from ingested food or commensal microbes (*1*, *2*). It is effective in preventing autoimmune diseases (e.g., arthritis, diabetes, and multiple sclerosis) and allergies (e.g., food allergy) in animal models (*3*). In humans, early exposure to peanut protein is reportedly capable of preventing peanut allergy in children (*4*, *5*). However, it has not been significantly successful in humans to induce oral tolerance for treating ongoing immunological diseases such as chronic allergy and autoimmune disease (*6*). It is therefore a long outstanding issue to determine how harmful immune responses that have been already triggered and chronically progressing can be halted and cured by inducing antigen-specific oral tolerance (*7*).

Naturally occurring $CD4^+$ regulatory T (nTreg) cells expressing the transcription factor Foxp3, including thymus-derived Treg (tTreg) cells and peripherally derived Treg (pTreg) cells, are indispensable for the induction and maintenance of immunological tolerance, including oral tolerance, and instrumental in controlling immunological diseases (*8–11*). It remains obscure, however, how antigen-specific pTreg cells are generated and how they establish and maintain oral tolerance(*2*). It has been suggested that, following antigen transportation through the intestinal epithelial cells, antigen-presenting cells (APCs), conventional dendritic cells (cDCs) in particular, play a pivotal role for the generation of antigen cognate pTreg cells in mesenteric lymph nodes (mLNs) and lymphoid tissues in the intestine (*12–14*). Intestinal cDCs can efficiently convert TGF-β into its active form, and vitamin A into retinoic acid (RA); TGF-β and RA synergistically induce intestinal pTreg cells upon antigen stimulation (*15–17*). These pTreg-inducing cDCs appear to be immature DCs with low expression of the costimulatory molecules CD80 and CD86 (*18–20*). However, the roles of CD28-mediated co-stimulation for pTreg generation and oral tolerance have not been well characterized. Addressing the issue, we have recently shown that *in vitro* antigen stimulation of conventional T (Tconv) cells in the presence of TGF-β and IL-2 but without CD28 signal is able to efficiently induce Foxp3 Treg cells equipped with Treg-specific epigenetic changes, hence Treg cell-lineage stability, and that such functionally stable *in vitro* induced Treg (iTreg) cells can be generated not only from naïve but also from effector/memory Tconv cells (*21*). The question then arises whether such *in vitro* generation of iTreg cells functionally similar to nTreg cells shares a common developmental basis with *in vivo* pTreg generation, especially in the context of oral tolerance.

Here, we have attempted to determine whether a functionally and phenotypically distinct type of pTreg cells are generated upon antigen exposure via the oral route, how they survive upon antigen stimulation and maintain their function to sustain oral tolerance, and how they can be exploited to establish robust oral tolerance not only in antigen-nonsensitized naïve mice but also in those that have been already antigen primed at other sites of the body.

Results

pTreg generation and maintenance by continuous antigen feeding and failure in establish-ing oral tolerance by prior antigen sensitization.

To analyze the development of pTreg cells by distinguishing them from tTreg cells, we used OVA-specific DO11.10 (DO) TCR transgenic mice that were made Rag2-deficient and expressing Foxp3-

eGFP reporter gene. DO Rag2KO Foxp3-eGFP mice thus produced are hereafter abbreviated as DORe mice. Foxp3$^+$ (i.e., GFP$^+$) cells were absent in the thymus, very few in the spleen and lymph nodes including mLNs in untreated DORe mice (see also below). To determine the effects of OVA feeding on anti-OVA T-cell responses in DORe mice, we kept feeding them for 4 weeks with the diet containing egg white powder (EWP) as 10% of the protein content or with control normal chow (NC), and assessed ear swelling after 4 times of tape stripping (TS) and papain/OVA treatment on the right ear and control TS/papain treatment on the left ear (**Fig. 1A**). Compared with NC-fed mice, which showed in the right ears severe ear swelling and histologically evident inflammation in the epidermis and dermis with abundant cellular infiltration, EWP-fed mice exhibited much lower degrees of ear swelling and histologically evident inflammation (**Fig. 1B** and **1C**). They had much smaller numbers of DO CD4$^+$ T cells (**Fig. S1A**) and much lower ratios of IFN-γ, IL-4, or IL-17A-producing DO CD4$^+$ T cells in the draining lymph nodes (dLNs) (**Fig. S1B**). They developed pTreg cells in mLNs, dLNs, and the right ear in much higher ratios compared with NC-fed mice (**Fig. 1D**). Treg cells were found to be present in the spleen and also in the control left ear as well at high ratios, although in small numbers (**Fig. S1C** and **1D**), with no significant ear swelling or inflammation in EWP-fed mice (Fig. **S1D** and **S1E**), suggesting systemic migration of the generated pTreg cells to various tissues. In addition, Diphtheria toxin (DTx) treatment of EWP-fed DO11.10 Rag2KO Foxp3-DTR-GFP (DORF) mice expressing the diphtheria toxin receptor (DTR) specifically in pTreg cells (**Fig. 1E**) depleted them in the OVA-challenged ear and dLNs and evoked severe ear swelling and inflammation (**Fig. 1F** and **1G**) with significant increases of inflammatory cytokine-producing T cells especially in the ear and dLNs (**Fig. S1F** and **S1G**).

To determine whether induction of oral tolerance would require continuous antigen exposure, we ceased EWP feeding for 4 or 8 weeks before the OVA challenge to the ear (**Fig. 1H**). Despite prior EWP feeding for 4 weeks, the feeding-suspended DORe mice showed ear inflammation as severe as control NC-fed mice (**Fig. 1I**), reduced ratios of pTreg cells, and increased cytokine-producing T cells in the ear tissue and dLNs when compared to DORe mice that had been kept EWP-fed until the ear testing (**Fig. 1J, S1H,** and **S1I**).

Next, to examine whether antigen-specific oral tolerance could be induced in precedingly antigen-primed mice, we first sensitized DORe mice by TS/papain/OVA treatment and then fed the mice with EWP or NC (**Fig. 1K**). Both groups developed similar degrees of ear swelling and inflammation (**Fig. 1L**). The frequencies of pTreg cells and Tconv cells producing inflammatory cytokines were comparable in mLNs, dLNs, and the ear tissues in both groups (**Fig. 1M, S1J,** and **S1K**). Moreover, the EWP-fed group showed significant body weight loss (**Fig. 1N**), indicating elicitation of systemic inflammation by oral antigen feeding in antigen-sensitized mice.

Collectively, continuous feeding of the diet containing protein antigen establishes antigen-specific oral tolerance by generating pTreg cells from antigen-specific Tconv cells. However, prior antigen sensitization at other sites or discontinuity of antigen feeding hampers oral tolerance induction and may even exacerbate an aberrant immune response upon antigen feeding.

Antigen-dependent development of pTreg cells with Treg type epigenome in oral tolerance.

To examine how the quality and quantity of antigens contained in the diet would affect the development and immunological characteristics of pTreg cells in oral tolerance, we fed DORe mice with the chow

containing various concentrations of EWP, antigen-free AIN-93G chow containing only casein as protein (*22*), or NC, starting from 2 weeks of age before weaning. EWP feeding increased the frequency of pTreg cells in mLNs and the small intestine lamina propria (SI-LP) in an antigen dose-dependent manner, even if antigen-containing chow was taken *ad libitum* (**Fig. 2A** and **2B**). High doses of EWP increased CD25 expression by the pTreg cells induced in SI-LP (**Fig. 2A** and **2C**), indicating their enhanced activation status (*23*). The EWP-induced pTreg cells were also maintained as $CD44^{hi}CD62L^{lo}$ effector/memory type T cells in SI-LP (**Fig. S2A** and **S2B**). These pTregs exhibited Treg-specific epigenetic modifications, including DNA hypomethylation at Treg signature gene loci, such as *Foxp3*-conserved non-coding sequence 2 (CNS2) region and other regions in *Ikzf2*, *Ikzf4*, and *Ctla4* loci (*24*) (**Fig. 2D**). By chromatin immunoprecipitation sequencing (ChIP-seq) of the genomic regions associated with histone H3 Lys27 acetylation (H3K27ac) as an indicator of active enhancer status, differential peak analysis revealed that Treg-specific enhancer regions were activated in pTreg cells from EWP-fed DORe mice, whereas Tconv-specific enhancer regions were not, as in nTreg cells in WT mice (*25*, *26*) (**Fig. 2E**). The pTreg cells thus generated had activated Treg-specific super-enhancers at the *Foxp3* gene locus and other Treg signature gene loci including *Ikzf2*, *Ikzf4*, *Ctla4*, and *Il2ra* as observed in WT-nTreg cells (**Fig. 2F** and **2G**). ATAC-seq further confirmed chromatin remodeling also in these loci (**Fig. 2F** and **2G**).

In the above experiments, we noted that NC-fed mice also possessed detectable numbers of pTreg cells in mLNs and SI-LP in particular, at higher frequencies than antigen-free- or 0% EWP chow-fed mice (**Fig. 2A** and **2B**). To analyze the finding, we compared pTreg development in DORe and WT mice after NC feeding, and found that the former developed $Foxp3^+$ cells at higher ratios than the latter in SI-LP, the large intestine lamina propria (LI-LP), and among small intestine intraepithelial (SI-IE) cells, but not in the spleen and LNs (**Fig. S2C** and **S2D**). The $Foxp3^+$ cells in NC-fed DORe mice exhibited DNA hypomethylation at Treg-specific demethylation regions in Treg signature genes (**Fig. S2E**), and expressed Helios and Neuropilin-1 (**Fig. S2F**), at comparable levels as WT nTreg cells. The results suggested that an antigen(s) cross-reactive with OVA in NC might activate DO Tconv cells to differentiate into functionally stable pTreg cells, although the number of the pTreg cells thus generated was not sufficient to induce OVA-specific oral tolerance (**Fig. 1B** and **1C**).

Taken together, these results indicate that the cognate antigen containing diet drives Tconv cells to differentiate into activated pTreg cells in the intestine, and enables them to acquire Treg-specific epigenetic changes, hence Treg-lineage stability similar to that of nTreg cells. In addition, the quantity of pTreg cells is dependent on the amount of the antigen contained in the diet; thus, more than a certain amount of the antigen is required for generating pTreg cells quantitatively sufficient for establishing oral tolerance.

Antigen feeding induces tissue-specific effector-type pTreg cells suppressing effector Tconv cell differentiation.

We next attempted to characterize the dynamics of the differentiation/activation of pTreg and Tconv cells in EWP-fed DORe mice using single-cell RNA-sequencing (scRNA-seq). Analysis of preprocessed 6,449 cells from four hash-tagged and pooled populations of DO^+ $CD4^+$ T cells (i.e., mLN or SI-LP cells in DORe mice NC- or 10% EWP-fed for 4 weeks) identified 13 clusters by the expression of T-lineage

signature genes (**Fig. 3A** and **S3A**). EWP feeding resulted in an increase of Cluster 8 (circulating 2), which was *Myb*^{hi} (indicative of augmented T-cell survival and exhaustion) (*27–29*), reductions of Cluster 4 (Teff-mix) and 11 (Th1), and conversion of Treg population from Cluster 5 to Cluster 3 in SI-LP (**Fig. 3B**). Compared to Cluster 5, Cluster 3 pTreg cells having increased after EWP feeding highly expressed activation-related genes (*Tnfrsf9*, *Tnfrsf4*, *Tigit,* and *Tnfrsf18*), Th2-type transcription factor (*Gata3*), and tissue repairing-related molecules (*Areg* and *Penk*) (**Fig. 3C**). In addition, SI-LP pTreg cells (Cluster 3 and 5) highly expressed *Ctla4* compared to mLN pTreg cells (Cluster 12) (**Fig. S3A** and **S3B**). Supporting these results, gene ontology analysis between Cluster 3 and 5 SI-LP pTreg cells revealed that Cluster 3 pTreg cells expressed highly activated and proliferative T cell phenotypes compared to Cluster 5 pTreg cells (**Fig. 3D**). To analyze further the kinetics of antigen-specific T cells in SI-LP, we re-clustered Cluster 3, 4, 5, and 11 based on commonalities and newly identified 8 clusters (**Fig. S3D, 3E-G,** and **S3E**). Together with pseudotime analysis (**Fig. 3G**), the analysis suggested that, among Foxp3^{+} cells (Clusters 0, 1, 4, 6, and 7), Clusters 0 and 7 became activated and differentiated upon EWP stimulation into Cluster 1 and 4, which expressed *Klrg1*, *Areg*, and *Penk*. Tconv cells (Clusters 2, 3, and 5) appeared to diminish effector T-cell populations with Th1 and Th17 gene signatures upon EWP feeding (**Fig. 3E**, **3F**, and **S3E**). *Mcl1*, an anti-apoptotic gene, was relatively high in *Sell*$^{+}$ (i.e., CD62L^{hi}) Foxp3^{+} cells (Cluster 7); *Bcl2* being high in Th1 cells (Cluster 5) (**Fig. S3F**).

We assessed protein expression to validate these findings by comparing EWP- and NC-fed SI-LP pTreg cells (**Fig. 3H-K**). The former showed significantly higher expression of 4-1BB (*Tnfrsf9*), OX40 (*Tnfrsf4*), and TIGIT (*Tigit*), in good correlations with their mRNA expression levels (**Fig. 3H** and **3I**). EWP-fed pTreg cells also contained increased proportions of GATA3^{+}, RORγt^{+}, or T-bet^{+} cells compared with NC-fed pTreg cells (**Fig. 3J** and **S3C**). High ratios of Foxp3^{+} to Foxp3^{-} cells expressing each transcriptional factor suggested the expansion of T-bet^{+} pTreg cells and GATA3^{+} ones by EWP feeding, and their suppression of T-bet^{+} and/or GATA3^{+} Tconv cells, or both (**Fig. 3J**). Furthermore, continuous EWP feeding induced Ki-67^{+} and KLRG1^{+} pTreg cells (i.e., highly proliferative and differentiated pTreg cells), which were significantly reduced in ratio after cessation of the feeding for 4 weeks (**Fig. 3K**).

We also conducted bulk mRNA-seq to assess the phenotype of pTreg cells in lymphoid and non-lymphoid tissues in EWP-fed mice. pTreg cells in mLNs and skin dLNs possessed more common features compared to those in SI-LP or the ear (**Fig. 3L** and **S4A**), suggesting that pTreg cells generated in the intestine underwent tissue-specific adaptation and acquired a tissue-specific Treg phenotype and function distinct from those of lymph node pTreg cells, as observed in scRNA-seq (**Fig. S4B**) (*30*). For example, SI-LP and ear-tissue pTreg cells (corresponding to Clusters 0, 1, 4, 6, and 7 in Fig. 3E) were distinct from LN pTreg cells in the expression of apoptosis-related molecules (**Fig. S4C**), for example, their lower expression of *Bcl2*, hence being more prone to die by apoptosis after their terminal differentiation (**Fig. 3M**). Further, among chemokine receptors controlling tissue migration, SI-LP and ear-tissue pTreg cells distinctly expressed CCR9 and CCR5, respectively, in both the mRNA and protein levels (**Fig. 3N, 3O,** and **S4D**).

Collectively, these results demonstrate that EWP feeding generates and sustain pTreg cells that can differentiate into tissue-specific effector-type Treg cells that suppress the differentiation/activation of effector Tconv cells.

Specific expression of CD101 by intestinal pTreg cells generated by antigen feeding.

We next searched for specific markers that could differentiate EWP-induced intestinal pTreg cells from other Treg cells, particularly from tTreg cells, by preparing mixed bone marrow chimeric (BMC) mice in which DORe BM-derived pTreg cells and WT (Thy1.1-eFox) mouse BM-derived nTreg cells developed in the same environment (**Fig. 4A**). While NC or 10% EWP feeding for 4 weeks from immediately after bone marrow transfer equally generated WT nTreg cells, only EWP feeding generated DORe BM-derived pTreg cells in mLNs, SI-LP, and SI-IE, and to lesser extents in popliteal LN and spleen, but not in the thymus (**Fig. 4B-4D**). Bulk mRNA-seq of DORe pTreg cells and WT nTreg cells in BMC mice having been EWP-fed for 8 weeks revealed the genes that were differentially expressed between the two Treg populations (**Fig. 4E**). Among such genes normalized for TPM (transcript per million) in the expression level, DORe-pTreg cells showed much higher expression of *Cd101* and *Gpr83* and lower expression of *Icos* when compared with WT nTreg cells from NC- or EWP-fed BMC mice (**Fig. 4F**). Regarding previously reported tTreg markers (*31*, *32*), *Ikzf2*(Helios) was low, whereas *Nrp1*(Neuropilin-1) was high, in DORe pTreg cells (**Fig. 4G**). Flowcytometric analysis further confirmed that DORe pTreg cells strongly expressed the CD101 protein in BMC mice (**Fig. 4H**). Similarly, in NC-fed WT (eFox) and DORe mice (**Fig. S2**), ~80% of DORe pTreg cells and ~25% of WT nTreg cells expressed CD101, while Foxp3^{-} Tconv cells scarcely expressed the molecule (**Fig. 4I** and **S5A-S5D**). In WT nTreg cells, CD101 expression was correlated well with the expression of activation-associated molecules such as Nrp-1, GITR, CD69, CD103, and CD44 especially in mLNs (**Fig. S5E** and **S5F**). Taken together, these results indicate that intestinal pTreg cells generated by antigen feeding are distinct from tTreg cells in the expression levels of certain genes, especially CD101.

***In vitro* induction of CD101^{+} iTreg cells from naïve and antigen-primed Tconv cells by blockade of costimulatory signal.**

Based on the above results, we investigated how functionally stable iTreg cells similar to CD101^{+} intestinal pTreg cells induced by antigen feeding could be generated *in vitro* from Tconv cells. Previous studies have shown that iTreg cells can be produced *in vitro* by anti-TCR stimulation with plate-bound anti-CD3 mAb in the presence of TGF-β, IL-2, and agonistic anti-CD28 mAb (*33*, *34*), and that, in the presence of IL-2, iTreg generation was more efficient in the absence of agonistic anti-CD28 mAb (*19*, *21*). Consistent with this, we found that iTreg cells generated without CD28 signal indeed expressed CD101 at higher levels than those produced with CD28 signal (**Fig. 5A** and **5B**). Moreover, CD28-deficient Tconv cells more efficiently differentiated into iTreg cells with higher expression of CD101 compared with CD28-intact Tconv cells; agonistic anti-CD28 mAb significantly hampered the generation of CD101^{+} iTreg cells from the latter, but not from the former (**Fig. 5C** and **5D**). Furthermore, TGF-β dose-dependent iTreg induction revealed that TGF-β significantly enhanced CD101 expression in a dose dependent manner only in iTreg cells generated without CD28 signal (**Fig. S6A**).

Next, to simulate *in vitro* the condition of intestinal pTreg generation in EWP-fed DORe mice, we examined the effects of CD80/CD86 blockade with CTLA-4-immunoglobulin (CTLA4-Ig) fusion protein on iTreg generation from naïve DORe Tconv cells stimulated with OVA in the presence of splenic DCs (**Fig. S6B**). CTLA4-Ig did not inhibit proliferative differentiation of Foxp3$^+$ cells even at high doses (**Fig. S6C**), increased CD101 expression levels in an IL-2 dependent fashion (**Fig. S6D**), and conferred *Foxp3*-CNS2 hypomethylation on the generated iTreg cells (**Fig. S6E**). With cDC1 and cDC2 cells prepared from SI-LP (**Fig. S7**), CTLA4-Ig in combination with all-trans retinoic acid (ATRA) significantly increased the generation of Foxp3$^+$ cells and enhanced their expression of CD101 on both types of DCs (**Fig. 5E** and **5F**). CTLA4-Ig together with ATRA increased iTreg generation and CD101 expression even in the presence of various inflammatory cytokines (**Fig. 5G**). Furthermore, with naïve or effector/memory Tconv cells from dLNs of OVA immunized DORe mice (**Fig. 5H**), CTLA4-Ig effectively augmented iTreg generation and their CD101 expression with naïve Tconv cells and, to lesser degrees, with effector/memory Tconv cells (**Fig. 5I** and **5J**).

Taken together, blockade of CD80/CD86 did not hamper iTreg generation with TGF-β, IL-2, and antigen stimulation, rather enhancing the generation of iTreg cells, CD101$^+$ ones in particular. Thus, CD28 signaling is dispensable for iTreg generation, especially in the presence of IL-2. CD101 expression could be attributed to the reduction of CD28 co-stimulatory signal in iTreg generation.

Establishment of oral tolerance in antigen-presensitized mice by CD80/CD86 blockade and subsequent antigen feeding.

The above result that CTLA4-Ig enabled iTreg cell induction from antigen-primed Tconv cells prompted us to determine whether *in vivo* CTLA4-Ig treatment would be able to establish oral tolerance even in precedingly antigen-primed mice (**Fig. 6A**). When DORe mice were OVA sensitized at the right ear, injected intraperitoneally (i.p.) with CTLA4-Ig at various doses or saline, and then fed with EWP chow for 4 days, the right ear swelling gradually subsided during the feeding whether the mice were treated with CTLA4-Ig or not (**Fig. S8A**). However, mice treated with saline or low-dose (2 mg) CTLA4-Ig showed significant weight loss during EWP feeding (**Fig. S8B**), contrasting with no weight loss in the mice CTLA4-Ig-treated at high (10 or 50 mg) doses. The weight loss recovered after cessation of the feeding (**Fig. 6B**). When these mice were OVA challenged to the left ear after 4-day EWP feeding, those treated with high dose (10 or 50 mg) CTLA4-Ig did not show ear swelling or succumb to histologically evident inflammation, contrasting with other groups suffering from severe ear swelling and dermatitis (**Fig. 6C** and **S8C**). Notably, contrasting with the CTLA4-Ig/EWP-treated mice exhibiting no ear swelling, the CTLA4-Ig/NC-treated mice developed severe ear swelling and dermatitis, indicating that both CTLA4-Ig and antigen feeding were required for inducing the unresponsiveness. There were little differences among these mouse groups in the ratio of Foxp3 cells on day 15 and 33, with a tendency of Treg increase in the CTLA4-Ig-treated mice (**Fig. 6D** and **6E**). The ratios of cytokine-secreting cells among DO Tconv cells were not significantly different among the mouse groups at day 15, except significant reduction of the ratio of IL-17$^+$ cells in dLNs of the CTLA4-Ig-treated groups compared with the saline-treated or NC-fed mice (**Fig. 6F**). IFNg$^+$ cells as well as IL-17$^+$ cells in the former were significantly lower compared with the latter at day 33 (**Fig. 6G**). The pTreg cells having developed in EWP-fed mice, whether treated with CTLA4-Ig or saline, showed Treg-specific DNA demethylation at

the *Foxp3* CNS2 region, suggesting their functional stability as Treg cells (**Fig. S8D**). Notably, CD101 expression was upregulated in Foxp3$^+$ cells at day 15 in the right ear and its dLNs of the CTLA4-Ig-treated mice depending on the dose of CTLA4-Ig, similarly in the left ear and its dLNs at day 33 (**Fig. 6H** and **6I**). Depletion of Foxp3$^+$ cells by DTx administration on day 15 and 18 in CTLA4-Ig-treated and then EWP-fed DORF mice resulted in an exacerbated ear inflammation, a decrease in pTreg cells within the inflamed ear tissue, and an increase in IL-4$^+$ T cells in dLNs (**Fig. 6J, S8E,** and **S8F**). CD101$^+$ Foxp3$^+$ cells were also significantly decreased in the inflamed ear tissue, dLNs and mLNs (**Fig. 6K**).

These results collectively demonstrate that CD80/CD86 blockade by CTLA4-Ig and subsequent antigen feeding is able to establish oral tolerance in antigen-presensitized mice through inducing CD101$^+$ pTreg cells.

Discussion

It has been controversial whether pTreg cells are as functionally stable as tTreg cells and how they can be functionally and phenotypically distinguished from the latter. We have shown here that intestinal pTreg cells induced by antigen feeding are similar to tTreg cells. They not only express Foxp3 but also possess Treg-type epigenetic changes such as DNA hypomethylation at the Treg-specific demethylation regions and activation of the Treg-specific super-enhancers at Treg signature gene loci including *Foxp3*, *Il2ra*, and *Ctla4*. Additionally, these cells display Helios^{hi} and Neuropilin-1^{hi} as are tTreg cells (*31*, *32*), while pTreg cells newly generated in BMC mice by EWP feeding were Helios^{low}. It is likely that chronic stimulation may gradually upregulate Helios and Neuropirin-1 in pTreg cells (*35*, *36*). In addition, the generated pTreg cells are in a terminally differentiated state as seen with tissue-specific and -resident tTreg cells, as illustrated by the expression of *Tnfrsf9*, *Tnfrsf4*, *Gata3*, and *Areg* as well as skin-specific chemokine receptors such as *Ccr5* and *Ccr8* (*30*, *37*). However, despite these immunological properties indicative of functional competence and stability of pTreg cells induced by antigen feeding, cessation of antigen administration resulted in decline of oral tolerance with diminution of proliferative and Bcl-2$^+$ (i.e., apoptosis resistant) pTreg cells. This could be, at least in part, attributed to the antigen specificity of the induced pTreg cells, as well as the strength and duration of antigen stimulation delivered to them in the periphery. tTreg cells are more self-reactive than Tconv cells, hence tonically stimulated in the periphery for better survival (*38*, *39*). In contrast, pTreg cells once generated by antigen feeding may recquire persistent or frequent stimulation by the administered cognate non-self antigen for their survival to maintain tolerance, despite their possession of Treg-specific epigenetic alterations and acquisition of tTreg-like immunological properties.

The generation of intestinal pTreg cells by antigen feeding depends on the quantity of cognate antigen contained in the diet. Notably, even DORe mice fed with NC or Ag-free diet developed Foxp3$^+$ T cells particularly in SI-LP and LI-LP, and that they are phenotypically and epigenetically indistinguishable from pTreg cells generated by EWP-high diet. In NC-fed mice, a certain diet protein(s) or a microbial substance(s) cross-reactive with OVA could likely stimulate DO Tconv cells to differentiate into pTreg cells. The NC-induced pTreg cells were, however, smaller in number and less activated (e.g., lower in CD25 expression) than the high-EWP-induced pTreg cells and unable to suppress ear swelling upon antigen exposure. These findings indicate that induction of oral tolerance

depends on the number of antigen-specific pTreg cells and/or their activation status, and that both events depend on the quantity of the ingested antigen. This dependency of oral tolerance on the quantity of administered antigen may also the case in establishing mucosal tolerance via other routes, for example, by sublingual antigen administration for allergy treatment (*40*).

Intestinal pTreg cells induced by antigen feeding specifically express CD101, which is also highly specific for iTreg cells generated *in vitro* by the absence or blockade of CD28 co-stimulatory signal. Intestinal pTreg cells found in NC-fed mice, as discussed above, also expressed CD101 whereas nTreg cells in mLNs in WT mice hardly expressed the molecule even after high-EWP feeding. Furthermore, *in vivo* treatment with CTLA4-Ig for oral tolerance induction generated $CD101^+$ pTreg cells in the antigen-challenged tissue; and the degree of the expression depended on the dose of CTLA4-Ig. Recent studies have shown that CD101 is highly expressed by tissue-resident Treg cells compared to circulating ones (*41*); its expression is correlated with the level of FOXP3 expression in human Treg cells (*42*), and with *in vivo* Treg suppressive capacity on GvHD and IBD in mouse models (*43*, *44*). CD101 is reportedly expressed by exhausted $CD8^+$ T cells as well (*45*). These findings when taken together suggest that CD101 plays a role in modulating TCR and CD28 signaling, especially the latter, required for pTreg development in the intestine and iTreg generation from Tconv cells, and likely their induction of anergy in the absence of CD28 signal. The molecular basis of the function of CD101 and its ligand, which is currently unknown, remains to be determined. Nevertheless, CD101 could be a useful marker for pTreg cells, especially those induced by $CD80/CD86^{low}$ tolerogenic DCs, which transduce TCR signal with reduced CD28 signal.

CD80/CD86 blockade by CTLA4-Ig facilitates *in vivo* $CD101^+$ pTreg induction and *in vitro* $CD101^+$ iTreg generation. The blockade and antigen stimulation allow both Treg populations to proliferate and enable them to acquire the Treg-type epigenome, hence their functional and cell-lineage stability (*21*). IL-2 is essential for this Treg generation because it can compensate for the absence or reduction of CD28 signaling, hampering anergy induction and enabling more efficient generation of iTreg cells than without the blockade. It is plausible that *in vivo* provision of IL-2 could further facilitate pTreg cell generation by antigen feeding after CD80/CD86 blockade. In addition, APCs, especially DCs, play key roles in pTreg cell induction by antigen feeding (*14*). Both cDC1 and cDC2 were able to generate iTreg cells *in vitro* under CD80/CD86 blockade. In addition to the role of CD80/CD86 for Treg induction by APCs, it has been shown that $PD\text{-}L1^+$ DCs are potent in inducing antigen-specific Treg cells and that PD-L1 blockade inhibits the induction (*46*, *47*). We and others have shown that Treg cells are able to inhibit the T-cell stimulatory activity of APCs by reducing their CD80/CD86 expression via trogocytosis and transendocytosis, which are dependent on Treg-expressed CTLA-4 (*48–51*). This CD80/CD86 reduction on APCs results in dissociation of PD-L1 from *cis*-bound CD80, increasing free-PD-L1 available for the inhibition of PD-1 expressing effector T cells (*51*). CTLA4-Ig can have a similar effect by disrupting *cis*-CD80-PD-L1 interaction depending on the ratio of CD80 to PD-L1 on APCs (*51–53*). We have shown in this report that reduction or abrogation of CD28 signal alone (for example, by utilizing CD28-deficient Tconv cells), without modulating PD-L1/PD-1 interaction, suffices to generate iTreg cells effectively. It still needs to be determined, however, whether enhanced

signaling from free-PD-L1 on APCs to PD-1$^+$ Tconv cells facilitates the conversion of the latter to pTreg cells.

Prior antigen sensitization and the following antigen feeding evoked systemic inflammation. CTLA4-Ig treatment before antigen feeding not only prevented the systemic inflammation but also suppressed local inflammation at the site of antigen exposure. These findings carry some clinical implications. First, it is conceivable that certain food allergy might be a consequence of prior antigen sensitization at other sites of the body, as proposed as the dual-allergen-exposure hypothesis for food allergy (*54*). Second, CTLA4-Ig has been used for treatment of allergy on the assumption that it may suppress effector T-cell activation and IgE production (*55*). We have shown here that CTLA4-Ig can additionally facilitate the generation of antigen-specific functionally stable pTreg cells from antigen-primed Tconv cells when combined with subsequent antigen feeding. Third, this approach to establishing oral tolerance by CD80/CD86 blockade and antigen feeding can be useful for mucosal tolerance induced by other ways, for example, by sublingual or subcutaneous antigen treatment to treat chronic allergy. It could also be extended to induction of immune tolerance towards microbial antigens derived from intestinal commensal bacteria to treat inflammatory bowel disease.

In conclusion, antigen-specific functionally stable CD101$^+$ pTreg cells are generated in the intestine by antigen feeding and engaged in the establishment of long-term systemic antigen-specific immune tolerance. CD101$^+$ iTreg cells with similar phenotype and function can also be produced *in vitro* from antigen-specific Tconv cells by depriving CD28 costimulation during their induction, suggesting a common developmental basis for these pTreg and iTreg cells. Furthermore, continuous antigen feeding combined with CD28 co-stimulation blockade is able to generate CD101$^+$ pTreg cells and establish immune tolerance even in previously antigen-sensitized animals.

Materials and methods

Study design

The main objective of this study was to determine how pTreg cells developed in the periphery, whether they formed a functionally stable Treg-lineage, and how they suppress antigen-specific inflammation. We fed TCR-monoclonal mice with antigen-containing diet to generate antigen-specific pTreg cells in the intestine. *In vivo* pTreg development was reproduced in two independent laboratories. A mouse model of delayed hypersensitivity was used to examine oral tolerance. Epigenetic status of pTreg cells was analyzed by bisulfite-seq, H3K27ac-ChIP-seq, and ATAC-seq. scRNA-seq analysis was performed to investigate pTreg and effector T-cell development under antigen-specific stimulation. We further assessed physiological pTreg development using mixed bone marrow chimeric mice. Gene expression profiles assessed by Bulk RNA-seq analysis were obtained from biological replicates. Using iTreg induction, we assessed favorable conditions to convert Tconv cells into Foxp3$^+$ cells. Sufficient numbers (more than three) of adult mice with matched ages (6 to 12 weeks) and both sexes were used for each *in vivo* and *in vitro* experiment.

Mice

BALB/c mice were purchased from SLC or CLEA. DO11.10 TCR transgenic mice, *Rag2*-deficient mice, Foxp3-eGFP (eFox) reporter mice, Thy1.1-eFox mice, Foxp3-DTR-GFP mice, and *CD28*-deficient mice

were previously described (*21*, *56*, *57*). All mice were maintained under specific pathogen-free conditions. All procedures were conducted in accordance with the National Institutes of Health Guide for the Care and Use of Laboratory Animals and approved by the Committee on Animal Research of Osaka University.

Food modification

AIN-93G diet and egg-white-powder (EWP)-added food were purchased from CLEA. AIN-93G diet was used as antigen-free food (**Table. 1**). CE-2 (CLEA) as normal chow (NC) was used as standard food in the animal facility. For DORe mice, food modification began at 2 weeks of age under milk feeding or at 4 weeks of age after weaning, and continued until 8 weeks of age. For bone marrow chimeric mice, the food modification was started at the time of bone marrow cell transfer, and continued for 4-8 weeks.

Epicutaneous sensitization of OVA antigen to mice

The procedure was described in previous studies (*58*). Mice were anesthetized with isoflurane. Both ears were treated with tape stripping five or six times using surgical tape (21N, Nichiban, Tokyo, Japan). Then, a total of 12.5 µl of 10 mg/ml of papain with 10 mg/ml OVA was applied to each side of the surface of mouse ear. This treatment was repeated twice per week for 2 weeks. During the experimental period, ear thickness was measured daily using a digital caliper. For depleting $Foxp3^+$ cells in the experiment, diphtheria toxin (400 ng in 200 µl PBS) was injected intraperitoneally twice per week into the Foxp3-DTR-GFP background mice.

Histopathology

Tissues were fixed with 10% formalin, embedded in paraffin blocks, and sectioned and stained by hematoxylin and eosin. For ear swelling test, histological and pathological scoring was performed by following criteria and summed up; disorder of epidermis: 1-3, disorder of dermis: 1-3, disorder of hypodermis: 1-3, cell invasion: 1-3, and range of inflammation: 1-3.

Isolation of ear-infiltrating immune cells

Dissected ears were minced into small pieces with scissors and digested in the isolation buffer (HBSS(−) with 2% FBS, 2 mg/ml Collagenase D (Roche), and 20 µg/ml DNaseI (Roche)) with 1,300 rpm shaking at 37℃ for 2 h. The suspension was then passed through a 70-µm mesh and mash the debris by using a syringe plunger. The flow-through was centrifuged at 500xg at 4℃ for 5 min. The pellet was washed and resuspended with FACS buffer. Isolated cells were used for flowcytometry directly or first stimulated with PMA and ionomycin in the presence of GolgiStop (BD) for 4 h at 37℃ for subsequent intracellular cytokine staining.

Isolation of lymphocytes from intestinal mucosa

Intestines were harvested from mice, the lumen was opened longitudinally with scissors, the luminal contents were removed, and the tissues were washed with FACS buffer. After cutting the tissues into 2 cm, they were incubated with IE isolation buffer (HBSS(−) with 2% fetal bovine serum (FBS), 1 mM EDTA (Nacalai)) at 37℃ for 30 min. The tissues were then incubated with LP isolation buffer (HBSS(−) with 2% FBS, 1 mg/ml collagenase D (Roche), and 10 µg/ml DNaseI (Roche)) at 37℃ for 30 minutes. The suspension was then passed through a 70-µm mesh, and the debris was mashed using a

syringe plunger. The flow-through was centrifuged at 500xg at 4°C for 5 min. The pellet was resuspended with 40% Percoll solution, then layered with 80% Percoll solution and centrifuged at 2,000 rpm at room temperature for 20 min without acceleration and brake. The interface was collected and washed with FACS buffer.

Generation of mixed bone marrow chimeric mice

Bone marrow cells were harvested from the femur and tibia of mice, using a 23G needle and syringe. After lysing red blood cells, CD3e^{+} T cells were removed using the MACS negative selection system (Miltenyi Biotec) or the BD IMag Cell Separation System (BD) following the manufacturer's protocol. T cell-depleted bone marrow cells from Thy1.1-eFox and DORe mice were mixed at a ratio of 1:2 in PBS buffer and injected intravenously into CD45.1^{+} *Rag2*-deficient mice as recipientsthat had been irradiated at 4.0 Gy. After 4 weeks or more later from bone marrow reconstitution, chimeric mice were sacrificed and analyzed.

Cell preparation, cell sorting, and flowcytometry

For the preparation of DORe-pTreg cells, CD4^{+}DO11.10^{+}CD25^{+}Foxp3-eGFP^{+} cells were sorted from the peripheral lymph nodes and peripheral tissues harvested from DORe mice. Peripheral Tconv cells were defined as these gating below; naïve Tconv cells (CD4^{+}CD25^{-}Foxp3-eGFP^{-}CD62L^{hi}CD44^{lo}) and effector Tconv cells (CD4^{+}CD25^{-}Foxp3-eGFP^{-}CD62L^{lo}CD44^{hi}). As antigen presenting cells, cDC1 (CD45^{+}CD11c^{+}IA-IE^{+}CD103^{+}CD11b^{-}) and cDC2 (CD45^{+}CD11c^{+}IA-IE^{+}CD103^{+}CD11b^{+}) fractions were sorted from SI-LP in CD45.1 WT mice. BD Cytofix/Cytoperm Fixation/Permeabilization Kit (BD) was used for intracellular staining for cytokines used following stimulation with PMA and Ionomycin and treatment with Golgi-Stop (BD Biosciences), and the Foxp3 staining kit (eBiosciences) was used for transcriptional factors or intracellular molecules. Flowcytometry analysis and cell sorting were performed using FACSCantoII, FACSCellesta, FACSAriaII, and FACSAriaFusion (BD Biosciences). Antibodies used in this study are listed (**Table S2**).

CpG methylation analysis by bisulfite sequencing in Treg-specific demethylation regions

Bisulfite sequencing analysis was performed as previously described (*59*). Briefly, cells were sorted by FACSAriaII, and gDNA was extracted by phenol extraction followed by ethanol precipitation. Bisulfite base conversion was carried out using the Methyl Easy Xceed Rapid DNA Bisulphite Modification Kit (Human Genetic Signatures) or following our original methods previously described. PCR primer sequences for Treg-specific demethylated regions are available (*24*, *59*).

ChIP-seq

ChIP-seq experiments were performed as previously described (*25*, *26*). Briefly, sorted cells were fixed with 1% formaldehyde (ThermoScientific) for 10 min for anti-histone ChIP at room temperature. After nuclear extraction, chromatin lysate was fragmentated using Picoruptor (Diagenode), 30 sec sonication and 30 sec cooling for 7 cycles at 4°C, before immunoprecipitation. Immunoprecipitated chromatin lysate was reverse cross-linked at 65°C for 24 h, followed by purification and library preparation using NGS Library Preparation kit for IonS5 (ThermoScientific) or NEBNext Ultra II DNA Library Prep Kit for Illumina (Illumina) according to the manufacturer's instructions. Raw data were generated using the IonS5 sequencing system (ThermoScientific) or NextSeq500 (Illumina).

ATAC-seq

ATAC-seq was performed as previously described (*60*). Briefly, sorted cells (up to 100,000 cells) were lysed with100 µl of lysis buffer (0.01% digitonin, 0.1% NP-40, 0.1% Tween 20 in resuspension buffer; 10 mM Tris-HCl pH7.5, 100 mM NaCl, 3 mM $MgCl_2$) for 3 min on ice. After removal of lysis buffer by centrifugation, Tn5 tagmentation was performed using Illumina Tagment DNA TDE1 Enzyme and Buffer Kits (Illumina) at 37°C for 30 min, with shaking at 1,000 rpm. After purification using DNA Clean & Concentrator-5 (Zymo Research), tagmented DNA was amplified using NEBNext High-Fidelity PCR Master Mix (New England BioLabs) with the following prepared DNA libraries were purified using DNA Clean & Concentrator-5 or Ampure XP (Beckman Coulter). Sequencing was performed using NextSeq500 or NovaSeq (Illumina).

Data processing and analyses of ChIP-seq and ATAC-seq data

For ChIP-seq analysis, raw sequence reads were inspected and trimmed using Trim-galore (v0.6.6) (Babraham Bioinformatics). Trimmed reads were mapped to mm10 genome using Bowtie2 (v2.3.5) (*61*) with the following options; --local --very-sensitive-local. Mapped reads were sorted using Samtools (v1.6)(*62*), then converted into bigwig files for visualization by bamCoverage (v3.1.3), included deepTools package(*63*), with the following options; -of bigwig --binSize 5 -p max --normalizeUsing CPM --smoothLength 15 –ignoreDuplicates. Peak calling was performed using MACS2 (v2.1.1.20160309)(*64*) with the following options; macs2 callpeak -t ${filename} -name ${outputfilename} -f BAM -g mm --SPMR --nolambda --nomodel --bdg --call-summits. For defining Treg or Tconv-specific enhancer regions, narrowPeak files were concatenated, sorted. Sorted narrowPeak file was merged using bedtools (v2.30.0)(*65*) and then converted into SAF format file. SAF peak file was annotated using HOMER (v4.11)(*66*). Count files were generated using featureCounts(*67*) with the following options; -a annotated.saf -F SAF -p -o counts.txt ${BAM}. Differential expression analysis was performed using DESeq2. To assess the tag density of H3K27ac signals in Treg and naïve Tconv cells, matrix files were created using computeMatrix (v3.1.3), included deepTools package, with the following options; --beforeRegionStartLength 2000 --regionBodyLength 5000 --afterRegionStartLength 2000 --skipZeros, then visualized plotProfile command.

For ATAC-seq analysis, sequence reads were mapped to mm10 genome using Bowtie2 (v2.3.5) by following options; --very-sensitive. Mapped reads were sorted by Samtools (v1.9) and then converted into bigwig files for visualization by bamCoverage (v3.1.3) with the following options; -of bigwig --binSize 5 -p max --normalizeUsing CPM --smoothLength 15 –ignoreDuplicates. Peak calling was performed using MACS2 (v2.1.1.20160309) with the following options; macs2 callpeak -t ${filename} -name ${outputfilename} -f BAM -g mm --SPMR --nolambda --nomodel --shift -75 --extsize 150 --keep-dup all --bdg --call-summits.

IGV Integrated genome viewer was used to visualize peak or region data.

Single-cell RNA-seq and analysis

Single-cell RNA-Seq was performed on a Chromium instrument (10X Genomics) following the user guide manual for 30 v3 or 50 v2 chemistry. Briefly, FACS-sorted DORe-derived T cells isolated from mLNs and SI-LP were stained with TotalSeq anti-mouse Hashtag Antibody (BioLegend), and washed

three times with FACS buffer. Cells were resuspended with FACS buffer to a final concentration of approximately 1,000 cells/µl with a viability above 90%. Capturing cells in droplets, reverse transcription, and cell barcoding were performed on the Chromium Controller (10x Genomics), followed by PCR amplification and library construction using Chromium Next GEM Single Cell 5' Kit v2. Final libraries were sequenced on NovaSeq6000 (Illumina), 20,000 reads/cell for mRNA and 5,000 reads/cell for antibody-derived tags.

Sequenced reads were quantified using Cell Ranger (v5.0.0) with the pre-built reference refdata-gex-mm10-2020-A downloaded from 10x Genomics' website. Quantified expressions were preprocessed and visualized using Seurat (v4.1.3 or v5.0.1)(*68*). Differentially expressed genes were calculated using "FindMarkers" function based on the non-parametric Wilcoxon rank sum test in Seurat. Gene ontology analysis was performed using clusterProfiler (v4.10.0)(*69*). For the trajectory analysis, selected cells were re-clustered and ordered using Monocle3 (v1.3.4)(*70*).

Bulk RNA-seq and analysis

Bulk RNA-seq was performed as below. Briefly, FACS-sorted cells were lysed by RLT RNA lysis buffer (Qiagen) containing 2-mercaptoethanol to a final concentration of approximately 1,000 cells/10 µl followed by reverse transcription using the SMART-seq v4 Ultra Low Input RNA Kit for Sequencing (Clontech). Library preparation was performed using the Kapa Library preparation kit for IonTorrent or for Illumina (KAPA) by following the manufacturer's protocol. Sequencing of cDNA libraries was performed on IonS5 (Thermo Scientific), NextSeq500, or NovaSeq6000 (Illumina).

Sequenced reads were inspected and trimmed using Trim-galore (v0.6.6) and aligned to the mouse genome GRCm38/mm10 using STAR (v2.7.7a)(*71*). Reads counts at the gene level were calculated using RSEM (v1.3.1)(*72*). Normalization for library size and differential expression analysis were performed using DESeq2 (v1.32.0)(*73*).

Cell culture

Cell culture was performed in RPMI 1640 supplemented with 10%(v/v) FBS, 60 g/ml penicillin G, 100 g/ml streptomycin, and 0.1 mM 2-mercaptoethanol. For in vitro Treg induction, sorted naïve Tconv cells were stimulated with plate-bound anti-CD3e mAb (clone: 145-2C11) and soluble anti-CD28 mAb (clone: 37.51) in the presence of 100 U/ml hIL-2 (Shionogi) and 5 ng/ml rhTGF-β_1 (R&D Systems). For the co-culture experiment, DORe-derived naïve Tconv cells were stimulated by sorted APCs, 5 µM $OVA_{323\text{-}339}$ peptide (MBL Co., LTD., MedChemExpress), 100 U/ml rhIL-2, and 2.5 ng/ml rhTGF-β_1 and with or without 10 nM ATRA supplementation (Wako) or 10 µg/ml CTLA4-Ig (abatacept; Orencia, BMS) for 72 hours.

Statistics

Values were expressed as mean ± SEM. Statistical significance was assessed by Student's *t* test or Welch's *t* test (two groups) following *F* test. One-way ANOVA and Tukey's HSD or Tukey-Kramer test were conducted for multiple comparisons. A p-value < 0.05 was considered statistically significant, and every p value was shown in the figures.

Supplementary Materials

Fig. S1. pTreg generation and maintenance by antigen feeding.
Fig. S2. Development of pTreg cells in NC-fed DORe mice.
Fig. S3. Single-cell RNA-seq analysis of T cells in DORe mice.
Fig. S4. Bulk mRNA-seq analysis of pTreg cells from different tissues after EWP feeding.
Fig. S5. CD101 expression by thymocytes and peripheral T cells in WT mice.
Fig. S6. Dose effects of CTLA-4-Ig, TGF-β, and IL-2 on iTreg generation.
Fig. S7. Gating strategy for isolating intestinal DCs.
Fig. S8. Effects of CD80/CD86 blockade and subsequent antigen feeding on antigen-presensitized mice.
Table S1. Nutrition facts of modified food
Table S2. List of antibodies

References and Notes

1. M. W. Chase, Inhibition of Experimental Drug Allergy by Prior Feeding of the Sensitizing Agent. *Experimental Biology and Medicine* **61**, 257–259 (1946).
2. V. Cerovic, O. Pabst, A. M. Mowat, The renaissance of oral tolerance: merging tradition and new insights. *Nat Rev Immunol*, doi: 10.1038/s41577-024-01077-7 (2024).
3. R. M. Rezende, H. L. Weiner, Oral tolerance: an updated review. *Immunology Letters* **245**, 29–37 (2022).
4. G. Du Toit, G. Roberts, P. H. Sayre, H. T. Bahnson, S. Radulovic, A. F. Santos, H. A. Brough, D. Phippard, M. Basting, M. Feeney, V. Turcanu, M. L. Sever, M. Gomez Lorenzo, M. Plaut, G. Lack, Randomized Trial of Peanut Consumption in Infants at Risk for Peanut Allergy. *N Engl J Med* **372**, 803–813 (2015).
5. G. Du Toit, M. F. Huffaker, S. Radulovic, M. Feeney, H. R. Fisher, M. Byron, L. Dunaway, A. Calatroni, M. Johnson, R.-X. Foong, A. Marques-Mejias, I. Bartha, M. Basting, H. A. Brough, C. Baloh, T. M. Laidlaw, H. T. Bahnson, G. Roberts, M. Plaut, L. M. Wheatley, G. Lack, for the Immune Tolerance Network LEAP-Trio Trial Team, Follow-up to Adolescence after Early Peanut Introduction for Allergy Prevention. *NEJM Evidence* **3** (2024).
6. A. M. C. Faria, H. L. Weiner, Oral tolerance. *Immunological Reviews* **206**, 232–259 (2005).
7. A. McI. Mowat, To respond or not to respond — a personal perspective of intestinal tolerance. *Nat Rev Immunol* **18**, 405–415 (2018).
8. T. Tanoue, K. Atarashi, K. Honda, Development and maintenance of intestinal regulatory T cells. *Nat Rev Immunol* **16**, 295–309 (2016).
9. D. Mucida, N. Kutchukhidze, A. Erazo, M. Russo, J. J. Lafaille, M. A. Curotto De Lafaille, Oral tolerance in the absence of naturally occurring Tregs. *Journal of Clinical Investigation* **115**, 1923–1933 (2005).
10. S.-W. Hong, P. D. Krueger, K. C. Osum, T. Dileepan, A. Herman, D. L. Mueller, M. K. Jenkins, Immune tolerance of food is mediated by layers of CD4+ T cell dysfunction. *Nature* **607**, 762–768 (2022).
11. S. Sakaguchi, N. Mikami, J. B. Wing, A. Tanaka, K. Ichiyama, N. Ohkura, Regulatory T Cells and Human Disease. *Annual Review of Immunology* **38**, 541–566 (2020).

12. E. Mazzini, L. Massimiliano, G. Penna, M. Rescigno, Oral Tolerance Can Be Established via Gap Junction Transfer of Fed Antigens from CX3CR1+ Macrophages to CD103+ Dendritic Cells. *Immunity* **40**, 248–261 (2014).
13. U. Hadis, B. Wahl, O. Schulz, M. Hardtke-Wolenski, A. Schippers, N. Wagner, W. Müller, T. Sparwasser, R. Förster, O. Pabst, Intestinal Tolerance Requires Gut Homing and Expansion of FoxP3+ Regulatory T Cells in the Lamina Propria. *Immunity* **34**, 237–246 (2011).
14. D. Esterházy, J. Loschko, M. London, V. Jove, T. Y. Oliveira, D. Mucida, Classical dendritic cells are required for dietary antigen–mediated induction of peripheral Treg cells and tolerance. *Nat Immunol* **17**, 545–555 (2016).
15. D. Mucida, Y. Park, G. Kim, O. Turovskaya, I. Scott, M. Kronenberg, H. Cheroutre, Reciprocal T_H 17 and Regulatory T Cell Differentiation Mediated by Retinoic Acid. *Science* **317**, 256–260 (2007).
16. C.-M. Sun, J. A. Hall, R. B. Blank, N. Bouladoux, M. Oukka, J. R. Mora, Y. Belkaid, Small intestine lamina propria dendritic cells promote de novo generation of Foxp3 T reg cells via retinoic acid. *The Journal of Experimental Medicine* **204**, 1775–1785 (2007).
17. J. L. Coombes, K. R. R. Siddiqui, C. V. Arancibia-Cárcamo, J. Hall, C.-M. Sun, Y. Belkaid, F. Powrie, A functionally specialized population of mucosal CD103+ DCs induces Foxp3+ regulatory T cells via a TGF-β– and retinoic acid–dependent mechanism. *The Journal of Experimental Medicine* **204**, 1757–1764 (2007).
18. A. E. Morelli, A. W. Thomson, Tolerogenic dendritic cells and the quest for transplant tolerance. *Nat Rev Immunol* **7**, 610–621 (2007).
19. M. J. Benson, K. Pino-Lagos, M. Rosemblatt, R. J. Noelle, All-trans retinoic acid mediates enhanced T reg cell growth, differentiation, and gut homing in the face of high levels of co-stimulation. *The Journal of Experimental Medicine* **204**, 1765–1774 (2007).
20. M. B. Lutz, R. A. Backer, B. E. Clausen, Revisiting Current Concepts on the Tolerogenicity of Steady-State Dendritic Cell Subsets and Their Maturation Stages. *The Journal of Immunology* **206**, 1681–1689 (2021).
21. N. Mikami, R. Kawakami, K. Y. Chen, A. Sugimoto, N. Ohkura, S. Sakaguchi, Epigenetic conversion of conventional T cells into regulatory T cells by CD28 signal deprivation. *Proceedings of the National Academy of Sciences of the United States of America* **117** (2020).
22. P. G. Reeves, F. H. Nielsen, G. C. Fahey, AIN-93 Purified Diets for Laboratory Rodents: Final Report of the American Institute of Nutrition Ad Hoc Writing Committee on the Reformulation of the AIN-76A Rodent Diet. *The Journal of Nutrition* **123**, 1939–1951 (1993).
23. M. Miyara, Y. Yoshioka, A. Kitoh, T. Shima, K. Wing, A. Niwa, C. Parizot, C. Taflin, T. Heike, D. Valeyre, A. Mathian, T. Nakahata, T. Yamaguchi, T. Nomura, M. Ono, Z. Amoura, G. Gorochov, S. Sakaguchi, Functional Delineation and Differentiation Dynamics of Human CD4+ T Cells Expressing the FoxP3 Transcription Factor. *Immunity* **30**, 899–911 (2009).
24. N. Ohkura, M. Hamaguchi, H. Morikawa, K. Sugimura, A. Tanaka, Y. Ito, M. Osaki, Y. Tanaka, R. Yamashita, N. Nakano, J. Huehn, H. J. Fehling, T. Sparwasser, K. Nakai, S. Sakaguchi, T Cell Receptor Stimulation-Induced Epigenetic Changes and Foxp3 Expression Are Independent and Complementary Events Required for Treg Cell Development. *Immunity* **37**, 785–799 (2012).

25. Y. Kitagawa, N. Ohkura, Y. Kidani, A. Vandenbon, K. Hirota, R. Kawakami, K. Yasuda, D. Motooka, S. Nakamura, M. Kondo, I. Taniuchi, T. Kohwi-Shigematsu, S. Sakaguchi, Guidance of regulatory T cell development by Satb1-dependent super-enhancer establishment. *Nature Immunology* **18**, 173–183 (2017).
26. R. Kawakami, Y. Kitagawa, K. Y. Chen, M. Arai, D. Ohara, Y. Nakamura, K. Yasuda, M. Osaki, N. Mikami, C. A. Lareau, H. Watanabe, G. Kondoh, K. Hirota, N. Ohkura, S. Sakaguchi, Distinct Foxp3 enhancer elements coordinate development, maintenance, and function of regulatory T cells. *Immunity* **54**, 947-961.e8 (2021).
27. J. Yuan, R. B. Crittenden, T. P. Bender, c-Myb Promotes the Survival of CD4+CD8+ Double-Positive Thymocytes through Upregulation of Bcl-xL. *The Journal of Immunology* **184**, 2793–2804 (2010).
28. S. Dias, A. D'Amico, E. Cretney, Y. Liao, J. Tellier, C. Bruggeman, F. F. Almeida, J. Leahy, G. T. Belz, G. K. Smyth, W. Shi, S. L. Nutt, Effector Regulatory T Cell Differentiation and Immune Homeostasis Depend on the Transcription Factor Myb. *Immunity* **46**, 78–91 (2017).
29. C. Tsui, L. Kretschmer, S. Rapelius, S. S. Gabriel, D. Chisanga, K. Knöpper, D. T. Utzschneider, S. Nüssing, Y. Liao, T. Mason, S. V. Torres, S. A. Wilcox, K. Kanev, S. Jarosch, J. Leube, S. L. Nutt, D. Zehn, I. A. Parish, W. Kastenmüller, W. Shi, V. R. Buchholz, A. Kallies, MYB orchestrates T cell exhaustion and response to checkpoint inhibition. *Nature* **609**, 354–360 (2022).
30. R. J. Miragaia, T. Gomes, A. Chomka, L. Jardine, A. Riedel, A. N. Hegazy, N. Whibley, A. Tucci, X. Chen, I. Lindeman, G. Emerton, T. Krausgruber, J. Shields, M. Haniffa, F. Powrie, S. A. Teichmann, Single-Cell Transcriptomics of Regulatory T Cells Reveals Trajectories of Tissue Adaptation. *Immunity* **50**, 493-504.e7 (2019).
31. A. M. Thornton, P. E. Korty, D. Q. Tran, E. A. Wohlfert, P. E. Murray, Y. Belkaid, E. M. Shevach, Expression of Helios, an Ikaros Transcription Factor Family Member, Differentiates Thymic-Derived from Peripherally Induced Foxp3+ T Regulatory Cells. *The Journal of Immunology* **184**, 3433–3441 (2010).
32. J. M. Weiss, A. M. Bilate, M. Gobert, Y. Ding, M. A. Curotto De Lafaille, C. N. Parkhurst, H. Xiong, J. Dolpady, A. B. Frey, M. G. Ruocco, Y. Yang, S. Floess, J. Huehn, S. Oh, M. O. Li, R. E. Niec, A. Y. Rudensky, M. L. Dustin, D. R. Littman, J. J. Lafaille, Neuropilin 1 is expressed on thymus-derived natural regulatory T cells, but not mucosa-generated induced Foxp3+ T reg cells. *Journal of Experimental Medicine* **209**, 1723–1742 (2012).
33. S. G. Zheng, J. D. Gray, K. Ohtsuka, S. Yamagiwa, D. A. Horwitz, Generation Ex Vivo of TGF-β-Producing Regulatory T Cells from CD4+CD25–Precursors. *The Journal of Immunology* **169**, 4183–4189 (2002).
34. W. Chen, W. Jin, N. Hardegen, K. Lei, L. Li, N. Marinos, G. McGrady, S. M. Wahl, Conversion of Peripheral CD4+CD25− Naive T Cells to CD4+CD25+ Regulatory T Cells by TGF-β Induction of Transcription Factor *Foxp3*. *The Journal of Experimental Medicine* **198**, 1875–1886 (2003).
35. E. Szurek, A. Cebula, L. Wojciech, M. Pietrzak, G. Rempala, P. Kisielow, L. Ignatowicz, Differences in Expression Level of Helios and Neuropilin-1 Do Not Distinguish Thymus-Derived from Extrathymically-Induced CD4+Foxp3+ Regulatory T Cells. *PLoS ONE* **10**, e0141161 (2015).

36. A. M. Thornton, E. M. Shevach, Helios: still behind the clouds. *Immunology* **158**, 161–170 (2019).
37. C. Schiering, T. Krausgruber, A. Chomka, A. Fröhlich, K. Adelmann, E. A. Wohlfert, J. Pott, T. Griseri, J. Bollrath, A. N. Hegazy, O. J. Harrison, B. M. J. Owens, M. Löhning, Y. Belkaid, P. G. Fallon, F. Powrie, The alarmin IL-33 promotes regulatory T-cell function in the intestine. *Nature* **513**, 564–568 (2014).
38. C.-S. Hsieh, Y. Liang, A. J. Tyznik, S. G. Self, D. Liggitt, A. Y. Rudensky, Recognition of the Peripheral Self by Naturally Arising CD25+ CD4+ T Cell Receptors. *Immunity* **21**, 267–277 (2004).
39. C.-S. Hsieh, H.-M. Lee, C.-W. J. Lio, Selection of regulatory T cells in the thymus. *Nat Rev Immunol* **12**, 157–167 (2012).
40. R. R. Windom, S. Seitz, J. B. Ly, N. Dunn, J. Fergeson, H. H. Windom, Food Sublingual Immunotherapy: Safety and Simplicity of a Real Food Updosing Protocol. *The Journal of Allergy and Clinical Immunology: In Practice* **12**, 2447-2453.e1 (2024).
41. A. Kaminski, F. T. Hager, L. Kopplin, F. Ticconi, A. Leufgen, E. Vendelova, L. Rüttger, G. Gasteiger, V. Cerovic, W. Kastenmüller, O. Pabst, M. Ugur, Resident regulatory T cells reflect the immune history of individual lymph nodes. *Sci. Immunol.* **8**, eadj5789 (2023).
42. A. Ferraro, A. M. D'Alise, T. Raj, N. Asinovski, R. Phillips, A. Ergun, J. M. Replogle, A. Bernier, L. Laffel, B. E. Stranger, P. L. De Jager, D. Mathis, C. Benoist, Interindividual variation in human T regulatory cells. *Proc. Natl. Acad. Sci. U.S.A.* **111** (2014).
43. I. Fernandez, R. Zeiser, H. Karsunky, N. Kambham, A. Beilhack, K. Soderstrom, R. S. Negrin, E. Engleman, CD101 Surface Expression Discriminates Potency Among Murine FoxP3+ Regulatory T Cells. *The Journal of Immunology* **179**, 2808–2814 (2007).
44. R. Schey, H. Dornhoff, J. L. C. Baier, M. Purtak, R. Opoka, A. K. Koller, R. Atreya, T. T. Rau, C. Daniel, K. Amann, C. Bogdan, J. Mattner, CD101 inhibits the expansion of colitogenic T cells. *Mucosal Immunology* **9**, 1205–1217 (2016).
45. W. H. Hudson, J. Gensheimer, M. Hashimoto, A. Wieland, R. M. Valanparambil, P. Li, J.-X. Lin, B. T. Konieczny, S. J. Im, G. J. Freeman, W. J. Leonard, H. T. Kissick, R. Ahmed, Proliferating Transitory T Cells with an Effector-like Transcriptional Signature Emerge from PD-1+ Stem-like CD8+ T Cells during Chronic Infection. *Immunity* **51**, 1043-1058.e4 (2019).
46. L. Wang, K. Pino-Lagos, V. C. De Vries, I. Guleria, M. H. Sayegh, R. J. Noelle, Programmed death 1 ligand signaling regulates the generation of adaptive Foxp3+ CD4+ regulatory T cells. *Proc. Natl. Acad. Sci. U.S.A.* **105**, 9331–9336 (2008).
47. L. M. Francisco, V. H. Salinas, K. E. Brown, V. K. Vanguri, G. J. Freeman, V. K. Kuchroo, A. H. Sharpe, PD-L1 regulates the development, maintenance, and function of induced regulatory T cells. *Journal of Experimental Medicine* **206**, 3015–3029 (2009).
48. K. Wing, Y. Onishi, P. Prieto-Martin, T. Yamaguchi, M. Miyara, Z. Fehervari, T. Nomura, S. Sakaguchi, CTLA-4 Control over Foxp3^{+} Regulatory T Cell Function. *Science* **322**, 271–275 (2008).
49. Y. Onishi, Z. Fehervari, T. Yamaguchi, S. Sakaguchi, Foxp3^{+} natural regulatory T cells preferentially form aggregates on dendritic cells *in vitro* and actively inhibit their maturation. *Proc. Natl. Acad. Sci. U.S.A.* **105**, 10113–10118 (2008).

50. O. S. Qureshi, Y. Zheng, K. Nakamura, K. Attridge, C. Manzotti, E. M. Schmidt, J. Baker, L. E. Jeffery, S. Kaur, Z. Briggs, T. Z. Hou, C. E. Futter, G. Anderson, L. S. K. Walker, D. M. Sansom, Trans-Endocytosis of CD80 and CD86: A Molecular Basis for the Cell-Extrinsic Function of CTLA-4. *Science* **332**, 600–603 (2011).
51. M. Tekguc, J. B. Wing, M. Osaki, J. Long, S. Sakaguchi, Treg-expressed CTLA-4 depletes CD80/CD86 by trogocytosis, releasing free PD-L1 on antigen-presenting cells. *Proc. Natl. Acad. Sci. U.S.A.* **118**, e2023739118 (2021).
52. E. P. Oxley, N. J. Kershaw, C. Louis, K. J. Goodall, M. M. Garwood, S. M. Jee Ho, V. T. F. Voo, H.-Y. Park, J. Iaria, L. L. L. Wong, A. G. Lebenbaum, S. Wiranata, E. S. Pang, E. S. J. Edwards, D. B. D'Silva, J. Hansen, M. C. Van Zelm, M. O'Keeffe, P. M. Hogarth, N. M. Haynes, N. D. Huntington, I. P. Wicks, R. A. Dickins, Context-restricted PD-(L)1 checkpoint agonism by CTLA4-Ig therapies inhibits T cell activity. *Cell Reports* **43**, 114834 (2024).
53. M. A. Robinson, A. Kennedy, C. T. Orozco, H.-C. Chen, E. Waters, D. Giovacchini, K. Yeung, L. Filer, C. Hinze, C. Lloyd, S. J. Dovedi, D. M. Sansom, Rigid, bivalent CTLA-4 binding to CD80 is required to disrupt the cis CD80/PD-L1 interaction. *Cell Reports* **43**, 114768 (2024).
54. G. Lack, Epidemiologic risks for food allergy. *Journal of Allergy and Clinical Immunology* **121**, 1331–1336 (2008).
55. F. Van Wijk, S. Hoeks, S. Nierkens, S. J. Koppelman, P. Van Kooten, L. Boon, L. M. J. Knippels, R. Pieters, CTLA-4 Signaling Regulates the Intensity of Hypersensitivity Responses to Food Antigens, but is Not Decisive in the Induction of Sensitization. *The Journal of Immunology* **174**, 174–179 (2005).
56. J. M. Kim, J. P. Rasmussen, A. Y. Rudensky, Regulatory T cells prevent catastrophic autoimmunity throughout the lifespan of mice. *Nature Immunology* **8**, 191–197 (2007).
57. A. Shahinian, K. Pfeffer, K. P. Lee, T. M. Kündig, K. Kishihara, A. Wakeham, K. Kawai, P. S. Ohashi, C. B. Thompson, T. W. Mak, Differential T Cell Costimulatory Requirements in CD28-Deficient Mice. *Science* **261**, 609–612 (1993).
58. S. Shimura, T. Takai, H. Iida, N. Maruyama, H. Ochi, S. Kamijo, I. Nishioka, M. Hara, A. Matsuda, H. Saito, S. Nakae, H. Ogawa, K. Okumura, S. Ikeda, Epicutaneous Allergic Sensitization by Cooperation between Allergen Protease Activity and Mechanical Skin Barrier Damage in Mice. *Journal of Investigative Dermatology* **136**, 1408–1417 (2016).
59. M. Arai, A. Fukuda, R. Morimoto, Y. Nakamura, Z. Ci, S. Sakaguchi, Protocol to evaluate cell lineage stability of mouse natural and induced regulatory T cells using bisulfite sequencing. *STAR Protocols* **3**, 101694 (2022).
60. M. R. Corces, A. E. Trevino, E. G. Hamilton, P. G. Greenside, N. A. Sinnott-Armstrong, S. Vesuna, A. T. Satpathy, A. J. Rubin, K. S. Montine, B. Wu, A. Kathiria, S. W. Cho, M. R. Mumbach, A. C. Carter, M. Kasowski, L. A. Orloff, V. I. Risca, A. Kundaje, P. A. Khavari, T. J. Montine, W. J. Greenleaf, H. Y. Chang, An improved ATAC-seq protocol reduces background and enables interrogation of frozen tissues. *Nature Methods* **14**, 959–962 (2017).
61. B. Langmead, S. L. Salzberg, Fast gapped-read alignment with Bowtie 2. *Nature Methods* **9**, 357–359 (2012).

62. H. Li, B. Handsaker, A. Wysoker, T. Fennell, J. Ruan, N. Homer, G. Marth, G. Abecasis, R. Durbin, The Sequence Alignment/Map format and SAMtools. *Bioinformatics* **25**, 2078–2079 (2009).
63. F. Ramírez, D. P. Ryan, B. Grüning, V. Bhardwaj, F. Kilpert, A. S. Richter, S. Heyne, F. Dündar, T. Manke, deepTools2: a next generation web server for deep-sequencing data analysis. *Nucleic Acids Research* **44**, W160–W165 (2016).
64. J. Feng, T. Liu, B. Qin, Y. Zhang, X. S. Liu, Identifying ChIP-seq enrichment using MACS. *Nature Protocols* **7**, 1728–1740 (2012).
65. A. R. Quinlan, I. M. Hall, BEDTools: A flexible suite of utilities for comparing genomic features. *Bioinformatics* **26**, 841–842 (2010).
66. S. Heinz, C. Benner, N. Spann, E. Bertolino, Y. C. Lin, P. Laslo, J. X. Cheng, C. Murre, H. Singh, C. K. Glass, Simple Combinations of Lineage-Determining Transcription Factors Prime cis-Regulatory Elements Required for Macrophage and B Cell Identities. *Molecular Cell* **38**, 576–589 (2010).
67. Y. Liao, G. K. Smyth, W. Shi, FeatureCounts: An efficient general purpose program for assigning sequence reads to genomic features. *Bioinformatics* **30**, 923–930 (2014).
68. Y. Hao, S. Hao, E. Andersen-Nissen, W. M. Mauck, S. Zheng, A. Butler, M. J. Lee, A. J. Wilk, C. Darby, M. Zager, P. Hoffman, M. Stoeckius, E. Papalexi, E. P. Mimitou, J. Jain, A. Srivastava, T. Stuart, L. M. Fleming, B. Yeung, A. J. Rogers, J. M. McElrath, C. A. Blish, R. Gottardo, P. Smibert, R. Satija, Integrated analysis of multimodal single-cell data. *Cell* **184**, 3573-3587.e29 (2021).
69. T. Wu, E. Hu, S. Xu, M. Chen, P. Guo, Z. Dai, T. Feng, L. Zhou, W. Tang, L. Zhan, X. Fu, S. Liu, X. Bo, G. Yu, clusterProfiler 4.0: A universal enrichment tool for interpreting omics data. *The Innovation* **2**, 100141 (2021).
70. J. Cao, M. Spielmann, X. Qiu, X. Huang, D. M. Ibrahim, A. J. Hill, F. Zhang, S. Mundlos, L. Christiansen, F. J. Steemers, C. Trapnell, J. Shendure, The single-cell transcriptional landscape of mammalian organogenesis. *Nature* **566**, 496–502 (2019).
71. A. Dobin, C. A. Davis, F. Schlesinger, J. Drenkow, C. Zaleski, S. Jha, P. Batut, M. Chaisson, T. R. Gingeras, STAR: Ultrafast universal RNA-seq aligner. *Bioinformatics* **29**, 15–21 (2013).
72. B. Li, C. N. Dewey, RSEM: accurate transcript quantification from RNA-Seq data with or without a reference genome. *BMC Bioinformatics* **12**, 323 (2011).
73. M. I. Love, W. Huber, S. Anders, Moderated estimation of fold change and dispersion for RNA-seq data with DESeq2. *Genome Biology* **15**, 1–21 (2014).

Acknowledgments
We thank all Sakaguchi lab members, particularly: R. Ishii and M. Matsuura for their technical assistance, C. Tay and S.K. Singh for critical reading of the manuscript. We would like to thank K. Kawade for advising us about the production of modified foods. The genomic sequencings and bioinformatic analysis were conducted using the facility at the Genome Information Research Center of the Research Institute for Microbial Diseases, Osaka University.

Funding
This study was supported by the Japan Society for the Promotion of Science (JSPS) grant-in-aid for JSPS Fellows (20J20443 to M.A.), JSPS Grant-in-Aid for Early-Career Scientists (20K16279 to R.K.), JSPS Grant-in-Aid for Scientific Research (23H02733 to R.K.), INFRONT Office of Director's Research Grants Program (to R.K.), Grant from Nipponham Foundation for the Future of Food (to R.K.), JSPS Grant-in-Aid for Specially Promoted Research (16H06295 to S.S.), JSPS Grant-in-Aid for Scientific Research (24H00610 to S.S.), and Leading Advanced Projects for Medical Innovation (LEAP; 18gm0010005 to S.S.).

Author contributions
M.A. initiated the study. M.A, R.K., N.M., and S.S. designed experiments. M.A., R.K., A.S., and T.K. performed food modification experiment. M.A., Yo.N., and D.M. performed scRNA-seq experiment. M.A. and Ya.N. performed library preparation with advice from N.O. M.A. analyzed all data. M.A. and S.S. wrote the manuscript.

Competing interests
The authors declare that they have no conflict of interest associated with this manuscript.

Data and materials availability
The raw data (fastq files) from ATAC-seq, ChIP-seq, RNA-seq, and scRNA-seq experiments have been deposited in the DDBJ BioProject database, with links to BioProject accession number PRJDB18773. All data needed to evaluate the conclusions in the paper are present in the paper or the Supplementary Materials.

Figure legends
Fig. 1. **pTreg generation and maintenance by antigen feeding in establishing oral tolerance.** (**A**) Antigen feeding to DORe mice and assessment of ear swelling upon antigen challenge. (**B**) Changes in right ear thickness in DORe mice treated as shown in (A). Arrowheads indicate OVA challenges. (**C**) Histology of right ear and histological scores in NC- or EWP-fed DORe mice. Bars in histology indicate 100 µm. (**D**) CD25 and Foxp3 expression by DO $CD4^+$ T cells in mLNs, dLNs, and both ears. Barplots indicate frequencies of $Foxp3^+$ cells (pTreg cells) (n = 10 and 11). (**E-G**) Treg cell depletion in EWP-fed DORF mice. Mice were treated twice with DTx followed by OVA challenge (E). Ear thickness and histological scores (F). Frequencies of pTreg cells in the right ear (G) (n = 5-7). (**H-J**) Cessation of EWP feeding for 4 weeks (designated EWP(-)4wk) or 8 weeks (EWP(-)8wk) before OVA challenge (H). Ear thickness and histological scores (I). Frequencies of pTreg cells in right ear (J) (n = 4-6). (**K-N**) Effects of skin OVA sensitization and subsequent OVA feeding on ear swelling upon OVA challenge (K). Ear

thickness and histological scores (L). Frequencies of pTreg cells in right ear (M) (n = 5 and 6). Changes in body weight of DORe mice (N). Vertical bars indicate mean ± SEM. Statistical significance was assessed by unpaired t test or Welch's t test (B, C, D, F, G, L, M, N), and Tukey-Kramer test (I, J).

Fig. 2. Antigen-dependent development of pTreg cells with Treg type epigenome in oral tolerance. (**A**) Representative CD25 and Foxp3 expression by DO CD4$^+$ T cells in mLNs and SI-LP from DORe mice maintained by designated diet for 6 weeks. (**B, C**) Frequencies of Foxp3$^+$ cells among DO CD4$^+$ T cells (B) and CD25 expression level of Foxp3$^+$ cells (C) in mLNs and SI-LP in the mouse groups as shown in (A) (n = 5-8). (**D**) Degrees of demethylation as percentage of demetylated CpG residues at Treg-specific demethylation regions in *Foxp3*-CNS2, *Ikzf2*, *Ikzf4*, and *Ctla4* loci of pTreg cells in the mice as shown in **A**. (**E**) H3K27ac ChIP-seq signals at global Treg-specific or Tconv-specific enhancer regions in WT or DORe-derived Tconv or Treg cells. (**F**, **G**) H3K27ac ChIP-seq and ATAC-seq peak call at the *Foxp3* gene locus (F) and other Treg-specific enhancer loci at *Ctla4*, *Il2ra*, and *Ikzf2* (G) in eFox-derived naïve Tconv and nTreg cells, DORe-derived naïve Tconv and pTreg cells. Vertical bars indicate mean ± SEM. Statistical significance was assessed by Tukey-Kramer test (B, C).

Fig. 3. Generation of tissue-specific effector-type pTreg cells by antigen feeding. (**A**) scRNA-seq of DO CD4$^+$ T cells in mice fed with NC- or EWP-food for 4 weeks from weaning. (**B**) Hashtag oligonucleotide (HTO) classification of DO CD4$^+$ T cells in SI-LP in NC- or EWP-fed mice (left) with proportion of cells in each cluster (right). (**C, D**) Volcano plot of differentially expressed genes (C) and gene ontology analysis (D) between Cluster 3 and 5 pTreg cells. (**E**) UMAP plots of cells re-clustered from Clusters 3, 4, 5, 11 shown in (A), with projection of specifically expressed genes. (**F**) UMAP plots with NC- or EWP-derived HTO and *Foxp3* expression, as shown in E. (**G**) Pseudotime trajectory of re-clustered cells in (F). (**H, I**) Contour plots and MFI of 4-1BB and OX40 (H), TIGIT and GITR (I) staining of pTreg cells in SI-LP of NC- or EWP-fed mice (n = 3-6). (**J**) Ratio of Foxp3$^+$ to Foxp3$^-$ cells in T-bet$^+$, GATA3$^+$, or RORγT$^+$ cells in NC- or EWP-fed mice (n = 4-6 each). (**K**) Ki-67 and KLRG1 expression of SI-LP-derived pTreg cells in DORe mice kept fed with NC or EWP, or ceased to be EWP-fed for 4 weeks （EWP (-)4wK） as shown in Fig. 1H (n = 4-5). (**L**) PCA of transcriptomes of pTreg cells from mLNs, dLNs, SI-LP, and ear tissue (n=3 each). (**M,** and **N**) TPM-normalized *Bcl2* (M), *Ccr9* and *Ccr5* (N) expression by pTreg cells from designated tissues. (**O**) CCR9 and CCR5 expression by SI-LP- and ear tissue-derived pTreg cells. Vertical bars indicate mean ± SEM. Statistical significance was assessed by unpaired t test or Welch's t test (H, I, J), and Tukey-Kramer test (K).

Fig. 4. Specific expression of CD101 by pTreg cells generated by antigen feeding. (**A**) Irradiated CD45.1 Rag2KO mice reconstructed with CD3e$^+$ cell-depleted bone marrow cells isolated from WT (Thy1.1-eFox) and DORe mice. Mixed BMC mice were analyzed at 4-8 weeks after BM cell transfer. (**B-D**) Representative flow cytometry profiles of WT- and DORe-derived CD4$^+$ T cells in mLNs of BMC mice fed with NC- or EWP-chow for 4 weeks (B). Frequency of WT- and DORe-derived Foxp3$^+$ cells in designated tissues (C) (n = 10-12) and in the thymus (n = 8) (D). (**E**) Volcano plot of differentially expressed genes between DORe-pTreg cells and WT-nTreg cells assessed by RNA-seq analysis. (**F, G**) TPM-normalized differentially expressed genes (F) and genes encoding known tTreg-markers (G) in BMC mice as shown in (B) (n = 3). (**H**) CD101 expression by DORe-pTreg cells and

WT nTreg cells in BMC mice as shown in (B). Barplots indicate MFI of CD101 expression and frequency of CD101$^+$ cells (n = 6). (**I**) CD101 expression by WT-Treg or Tconv cells, DORe-pTreg or Tconv cells in untreated mice. Barplots indicate MFI of CD101 expression and frequency of CD101$^+$ cells (n = 3). Vertical bars indicate mean ± SEM. Statistical significance was assessed by unpaired t test or Welch's t test (C, H).

Fig. 5. *In vitro* generation of CD101$^+$ iTreg cells by absence or blockade of costimulatory signal during their induction. (**A**) *In vitro* iTreg generation and their CD101 expression. iTreg cells were induced by plate-bound anti-CD3e mAb with or without anti-CD28 mAb in the presence of TGF-β and IL-2 (n = 3). (**B**) iTreg induction and their CD101 expression by anti-CD3e (0.5, 1, 5, and 10 μg/ml) and anti-CD28 mAb (0, 0.5, 1, and 2 μg/ml) stimulation as in (A) (n = 3). (**C**, **D**) iTreg induction from CD28-deficient or -intact CD4$^+$ T cells (C) and their expression of CD101 (D) as in (A) (n = 3). (**E**, **F**) iTreg generation (E) and CD101 expression (F) by iTreg cells induced by co-culturing DO naïve Tconv cells with SI-LP-derived cDC1 or cDC2 in the presence of OVA and CTLA4-Ig (n = 4). (**G**) Effects of inflammatory cytokines (10 ng/ml each) and CTLA4-Ig on antigen-specific iTreg induction and their CD101 expression as in (E) and (F) (n = 3). 1 and 2 mean cDC1 and cDC2, respectively. (**H**) iTreg induction from antigen-specific Tconv cells in antigen-sensitized DORe mice. Naïve or effector Tconv cells from dLNs of antigen-sensitized DORe mice were co-cultured with SI-LP-derived cDC1 or cDC2 cells in the presence of OVA and CTLA4-Ig. (**I, J**) Frequencies of iTreg cells (I) and CD101 expression (J) of iTreg cells induced as shown in (H) (n = 6). Vertical bars indicate mean ± SEM. Statistical significance was assessed by Tukey's HSD test (B) and unpaired t test or Welch's t test (C, D, E, F, G, J).

Fig. 6. Establishment of oral tolerance in antigen-presensitized mice by CD80/CD86 blockade and subsequent antigen feeding. (**A**) Experimental protocol. DORe mice were OVA sensitized at the right ear four times, i.p. injected with CTLA4-Ig or saline on day 11, fed with EWP chow or NC for four days, OVA challenged at the left ear four times from day 22, and assessed for ear swelling on day 32. Body weight was also measured during these treatments. (**B, C**) Changes in body weight (B), left ear thickness and histological scores (C) (n=5). Arrowheads indicate OVA challenges. (**D**, **E**) Frequencies of pTreg cells in mLNs, dLNs, and the right ear at day 15 (D) and day 33 (E) (n=5).. (**F**, **G**) Frequencies of IFN-γ$^+$, IL-4$^+$, and IL-17A$^+$ cells in dLNs at day 15 (F) and day 33 (G) (n = 5-6). (**H**) CD101 expression by pTreg cells in dLNs and the right ear at day 15. Numbers in the histogram are representative of the frequency of CD101$^+$ cells. Barplots indicate the frequency of CD101$^+$ pTreg cells (n = 4-10/group). (**I**) Frequencies of CD101$^+$ pTreg cells in dLNs and the left ear at day 33 (n = 5-6). (**J**, **K**) Effects of Treg depletion after CTLA4-Ig injection and EWP feeding, After CTLA4-Ig injection and EWP feeding, DORF mice were i.p. treated with PBS or DTx at days 15 and 18, and re-challenged with OVA (arrowheads). Changes in left ear thickness at day 33 in DORF mice (J) (n = 6-7). CD101 expression by pTreg cells in mLNs, dLNs, and the left ear (K). Barplots indicate the frequencies of CD101$^+$ pTreg cells (n = 3). Vertical bars indicate mean ± SEM. Statistical significance was assessed by Tukey-Kramer test (C, D, E, F, G, H, I) and unpaired t test or Welch's t test (J, K).

Fig. S1. pTreg generation and maintenance by antigen feeding. (**A**) The number of DO $CD4^+$ T cells in dLNs in Fig. 1A. (**B**) Frequency of IFN-γ^+, IL-4^+, and IL-$17A^+$ cells among DO $CD4^+$ T cells in dLNs (*n* = 10 and 11). (**C**) CD25 and Foxp3 expression by DO $CD4^+$ T cells in the spleen at 4 weeks after designated feeding (*n* = 4). (**D**) Changes in left ear thickness in Fig. 1A. Arrowheads indicate OVA challenges. (**E**) Histology and histological scores of the left ear in NC- and EWP-fed DORe mice. Bars in histology indicate 100 µm. (**F**, **G**) Frequencies of pTreg cells in mLNs, dLNs, and the right ear (F) and frequencies of IFN-γ^+, IL-4^+, and IL-$17A^+$ cells in dLNs (G) in the mice shown in Fig. 1G (*n* = 7 (PBS-treated) or *n* = 6 (DTx-treated)). (**H**, **I**) Frequencies of pTreg cells in mLNs and dLNs (H), and frequencies of IFN-γ^+, IL-4^+, and IL-$17A^+$ cells in dLNs (I) in the mice shown in Fig. 1J (*n* = 4-6). (**J**, **K**) Frequencies of pTreg cells in mLNs and dLNs (J), and frequencies of IFN-γ^+, IL-4^+, and IL-$17A^+$ cells in dLNs (K) (*n* = 4-6). Vertical bars indicate mean ± SEM. Statistical significance was assessed by unpaired *t* test or Welch's *t* test (A, B, C, E, F, G, J, K), and Tukey-Kramer test (H, I).

Fig. S2. Development of pTreg cells in NC-fed DORe mice. (**A**, **B**) CD62L and CD44 expression by pTreg cells (A) and frequencies of $CD44^{hi}CD62L^{lo}$ effector pTreg cells (B) in mLNs and SI-LP from DORe mice fed with designated diet for 6 weeks. (**C**) Representative data of DO $CD4^+$ T cells in lymphoid tissues and peripheral tissues harvested from NC-fed DORe mice in comparison to NC-fed Foxp3-eGFP (eFox) mice. (**D**) Frequencies of $CD25^+Foxp3^+$ T cells in the thymus and $Foxp3^+$ T cells in various tissues (n=3 for thymus, spleen, pLNs, mLNs, and Peyer's patches (PP)) or (*n* = 6 for SI-IE, SI-LP, and LI-LP). (**E**) Methylation status in TSDRs of DORe-derived pTreg cells compared to eFox-derived nTreg cells. Empty and black circles indicate demethylated and methylated CpG residues, respectively. (**F**) Helios and Nrp-1 expression levels of eFox-Tconv, DORe-Tconv, eFox-nTreg, and DORe-pTreg cells. Barplots indicate MFI of Helios and Nrp-1 expression on eFox-nTreg cells and DORe-pTreg cells (*n* = 3). Vertical bars indicate mean ± SEM.

Fig. S3. Single-cell RNA-seq analysis of T cells in DORe mice. (**A**) Uniform manifold approximation and projection (UMAP) plots for expression levels of T cell-related molecules in DO $CD4^+$ T cells in NC- or EWP-fed DORe mice. (**B**) Volcano plot of genes differentially expressed between Cluster 12 and 5 pTreg cells. (**C**) GATA3, RORγT, and T-bet expression and frequency of pTreg and $Foxp3^-$ cells expressing each transcriptional factor. Cells were isolated from SI-LP in NC- or EWP-fed mice (*n* = 4-6) as in Fig.3F. (**D**) Upsetplot of DORe T-cell fractions detected by scRNA-seq clustering. Connected dots indicate intersections among clusters. (**E**) Marker dotplots of differentially expressed genes in re-clustered T cell clusters in Fig. 3E. (**F**) Marker dotplots of anti-apoptosis and pro-apoptosis related genes in re-clustered T cell clusters. Vertical bars indicate mean ± SEM. Statistical significance was assessed by unpaired *t* test or Welch's *t* test (C).

Fig. S4. Bulk mRNA-seq analysis of pTreg cells from different tissues after EWP feeding. (**A**) Heatmap of normalized counts of top 100 differentially expressed genes assessed by bulk RNA-seq in Fig. 3L. (**B**) Projection of 75 Cluster 3-up-regulated genes detected by scRNA-seq as shown in Fig. 3C on the transcriptome. (**C**) Heatmap of anti-apoptosis and pro-apoptosis related genes among pTreg cells from designated tissues. (**D**) TPM-normalized gene expression of chemokine receptors among DORe-pTreg cells derived from different tissues. Vertical bars indicate mean ± SEM.

Fig. S5. CD101 expression by thymocytes and peripheral T cells in WT mice. (**A**, **B**) Representative gating strategy of thymocytes in WT mice (A). Representative histogram of CD101 expression and frequencies of $CD101^+$ cells in WT thymus-derived T-cell fractions (B) (n = 4). Numbers in the histogram are representative of the frequencies of $CD101^+$ cells. (**C**, **D**) Representative gating strategy of mLN-derived cells in WT mice (C). Representative histogram of CD101 expression and frequencies of $CD101^+$ cells in WT mLN-derived T-cell fractions (D) (n = 6). Numbers in the histogram are representative of the frequencies of $CD101^+$ cells. (**E**, **F**) Representative flowcytometry profiles of CD101 and T cell-related molecules on $Foxp3^+$ Treg or $Foxp3^-$ T cells from the thymus (E) and mLNs (F). Vertical bars indicate mean ± SEM.

Fig. S6. Dose effects of CTLA-4-Ig, TGF-β, and IL-2 on iTreg generation. (**A**) Synergistic effect of TGF-β supplementation and CD28 signal deprivation on *in vitro* iTreg induction and CD101 expression by naïve $CD4^+$ Tconv cells (n = 4). (**B**) Experimental design. DORe-derived naïve Tconv cells and splenic DCs were co-cultured with or without CTLA4-Ig in the presence of OVA, TGF-β and IL-2. (**C**) Response to various concentrations of CTLA4-Ig (0, 2, 10, and 50 μg/ml) in *in vitro* iTreg induction (n = 4). (**D**) Response to various concentrations of IL-2 (0, 1, 10, and 100 U/ml) in *in vitro* iTreg induction and CD101 expression (n = 4 (0 U/ml) and n = 7 (1-100 U/ml)). (**E**) Degrees of demethylation as percentage at *Foxp3*-CNS2 regions of iTreg cells induced with or without CTLA4-Ig. Vertical bars indicate mean ± SEM. Statistical significance was assessed by unpaired t test or Welch's t test (A, C).

Fig. S7. Gating strategy for isolating intestinal DCs. Gating strategy for isolating classic dendritic cells from SI-LP of WT mice.

Fig. S8. Effects of CD80/CD86 blockade and subsequent antigen feeding on antigen-presensitized mice. (**A**, **B**) Changes in ear thickness and histological scores (A). Changes in body weight of DORe mice from day 0 to 15 in the experiment in Fig. 6A. (B). Arrowheads indicate OVA challenge.s (**C**) Histology of the left ear at day 33 shown in Fig. 6C. Bars in histology indicate 100 μm. (**D**) Demethylation status and frequencies of demethylation at *Foxp3*-CNS2 locus of DORe pTreg cells isolated from the mice treated with saline or 10 μg CTLA4-Ig followed by EWP feeding and assessed at day 15 in Fig. 6A. (**E-F**) Frequencies of pTreg cells in mLNs, dLNs, and left ears (E) and of IFN-γ^+, IL-4^+, and IL-$17A^+$ cells in dLNs at day 33 in DORF mice treated as described in Fig. 6J (F) (n = 6-7). Vertical bars indicate mean ± SEM. Statistical significance was assessed by unpaired t test or Welch's t test (E, F).

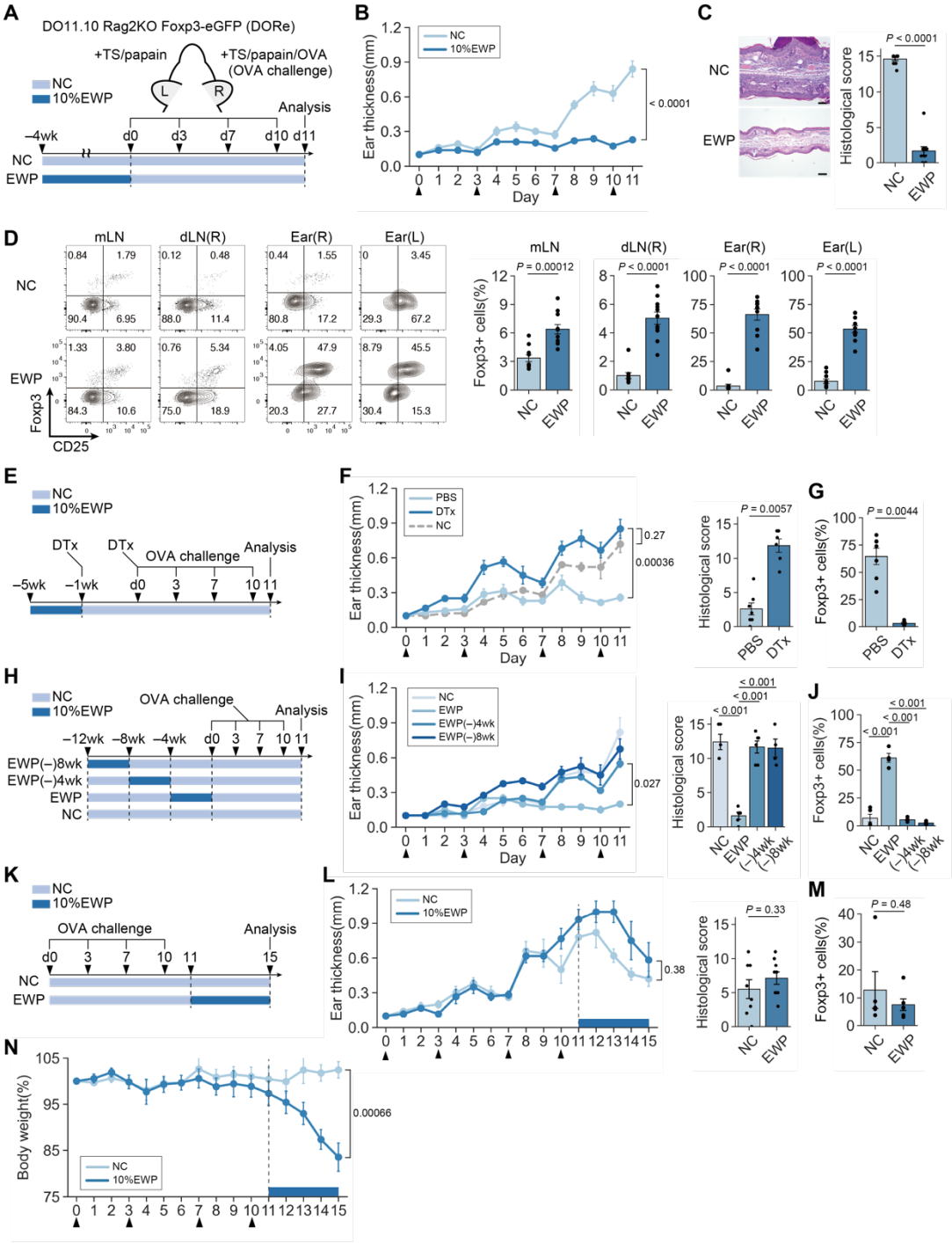
A
DO11.10 Rag2KO Foxp3-eGFP (DORe)
+TS/papain
+TS/papain/OVA (OVA challenge)
NC
10%EWP
L
R
Analysis
–4wk
d0
d3
d7
d10
d11
B
Ear thickness(mm)
Day
< 0.0001
C
P < 0.0001
Histological score
D
mLN
dLN(R)
Ear(R)
Ear(L)
Foxp3
CD25
Foxp3+ cells(%)
P = 0.00012
P < 0.0001
E
DTx
OVA challenge
–5wk
–1wk
F
PBS
DTx
0.27
0.00036
P = 0.0057
G
P = 0.0044
H
–12wk
–8wk
EWP(–)8wk
EWP(–)4wk
I
EWP(–)4wk
EWP(–)8wk
0.027
< 0.001
J
K
L
0.38
P = 0.33
M
P = 0.48
N
Body weight(%)
0.00066

Fig. 1

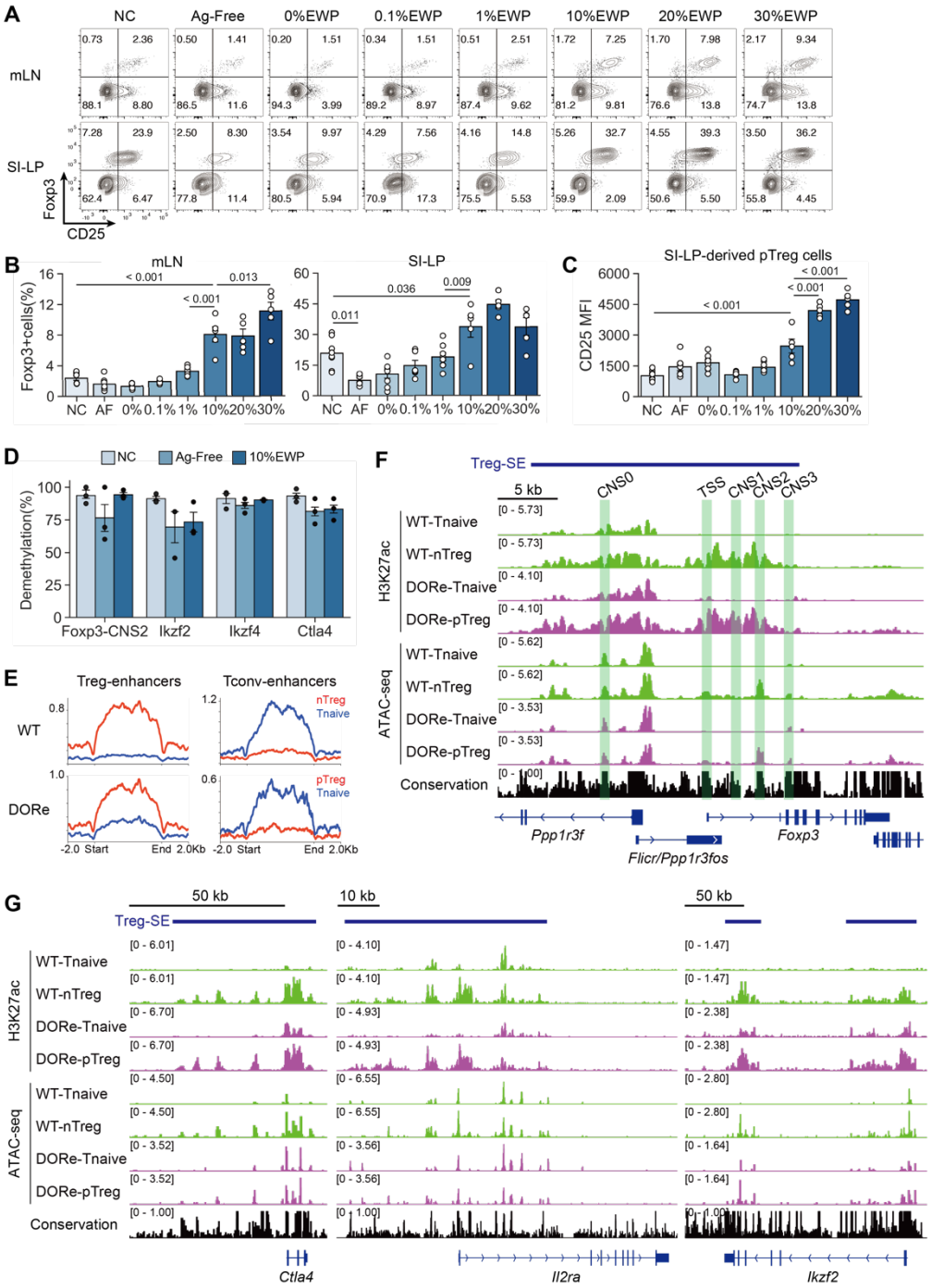
A
NC
Ag-Free
0%EWP
0.1%EWP
1%EWP
10%EWP
20%EWP
30%EWP
mLN
SI-LP
Foxp3
CD25
B
mLN
SI-LP
Foxp3+cells(%)
NC AF 0% 0.1% 1% 10% 20% 30%
C
SI-LP-derived pTreg cells
CD25 MFI
D
NC
Ag-Free
10%EWP
Demethylation(%)
Foxp3-CNS2
Ikzf2
Ikzf4
Ctla4
E
Treg-enhancers
Tconv-enhancers
WT
DORe
nTreg
Tnaive
pTreg
Tnaive
-2.0 Start
End 2.0Kb
F
Treg-SE
5 kb
CNS0
TSS
CNS1
CNS2
CNS3
H3K27ac
ATAC-seq
WT-Tnaive
WT-nTreg
DORe-Tnaive
DORe-pTreg
Conservation
Ppp1r3f
Flicr/Ppp1r3fos
Foxp3
G
50 kb
10 kb
50 kb
Treg-SE
Ctla4
Il2ra
Ikzf2

Fig. 2

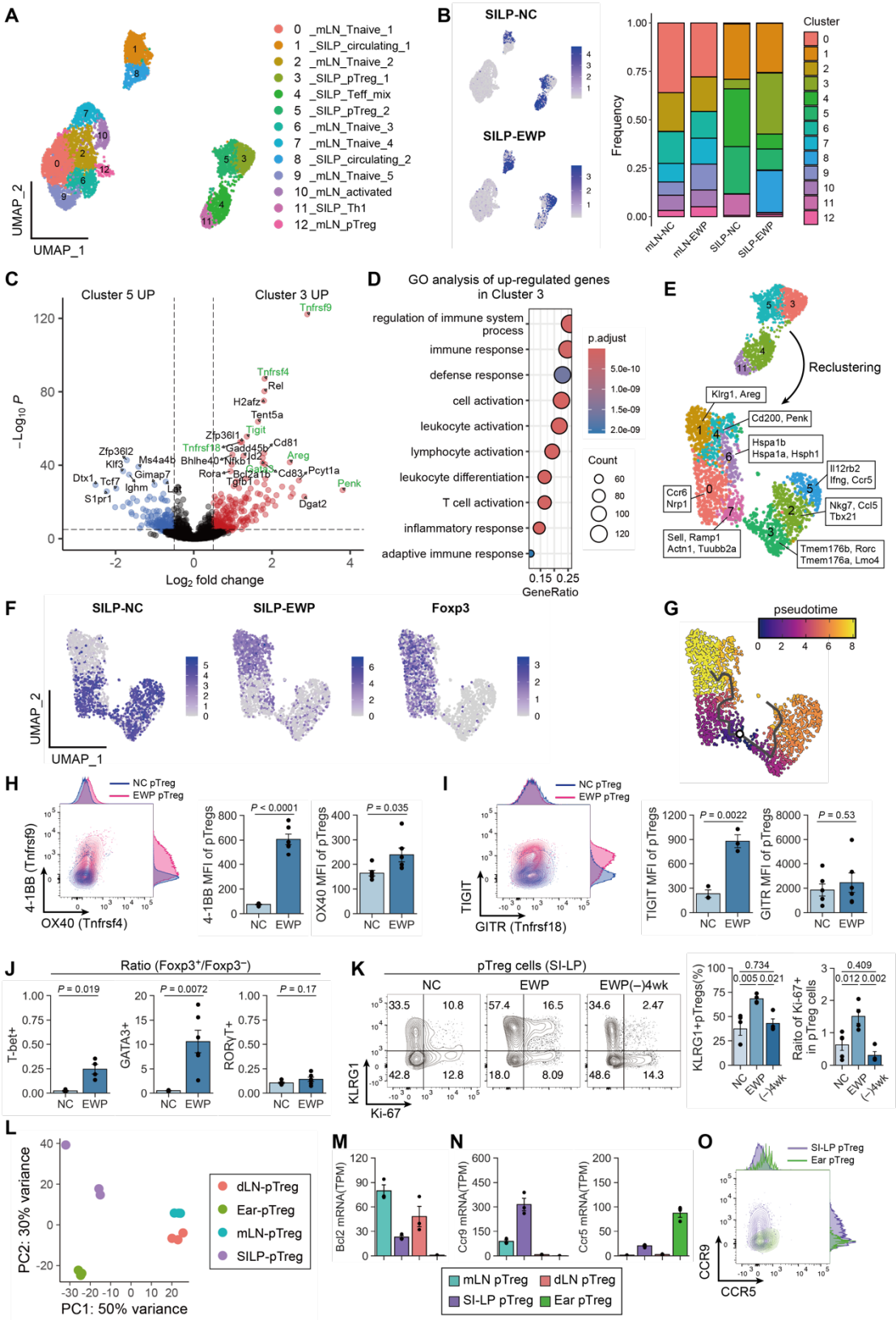
A
0 _mLN_Tnaive_1
1 _SILP_circulating_1
2 _mLN_Tnaive_2
3 _SILP_pTreg_1
4 _SILP_Teff_mix
5 _SILP_pTreg_2
6 _mLN_Tnaive_3
7 _mLN_Tnaive_4
8 _SILP_circulating_2
9 _mLN_Tnaive_5
10 _mLN_activated
11 _SILP_Th1
12 _mLN_pTreg
UMAP_2
UMAP_1
B
SILP-NC
SILP-EWP
Frequency
Cluster
mLN-NC
mLN-EWP
SILP-NC
SILP-EWP
C
Cluster 5 UP
Cluster 3 UP
Log2 fold change
D
GO analysis of up-regulated genes in Cluster 3
regulation of immune system process
immune response
defense response
cell activation
leukocyte activation
lymphocyte activation
leukocyte differentiation
T cell activation
inflammatory response
adaptive immune response
p.adjust
Count
GeneRatio
E
Reclustering
Klrg1, Areg
Cd200, Penk
Hspa1b
Hspa1a, Hsph1
Il12rb2
Ifng, Ccr5
Ccr6
Nrp1
Nkg7, Ccl5
Tbx21
Sell, Ramp1
Actn1, Tuubb2a
Tmem176b, Rorc
Tmem176a, Lmo4
F
SILP-NC
SILP-EWP
Foxp3
UMAP_2
UMAP_1
G
pseudotime
H
NC pTreg
EWP pTreg
4-1BB (Tnfrsf9)
OX40 (Tnfrsf4)
4-1BB MFI of pTregs
OX40 MFI of pTregs
P < 0.0001
P = 0.035
NC
EWP
I
NC pTreg
EWP pTreg
TIGIT
GITR (Tnfrsf18)
TIGIT MFI of pTregs
GITR MFI of pTregs
P = 0.0022
P = 0.53
J
Ratio (Foxp3+/Foxp3−)
T-bet+
GATA3+
RORγT+
P = 0.019
P = 0.0072
P = 0.17
K
pTreg cells (SI-LP)
NC
EWP
EWP(−)4wk
KLRG1
Ki-67
KLRG1+pTregs(%)
Raito of Ki-67+ in pTreg cells
L
PC2: 30% variance
PC1: 50% variance
dLN-pTreg
Ear-pTreg
mLN-pTreg
SILP-pTreg
M
Bcl2 mRNA(TPM)
N
Ccr9 mRNA(TPM)
Ccr5 mRNA(TPM)
mLN pTreg
dLN pTreg
SI-LP pTreg
Ear pTreg
O
SI-LP pTreg
Ear pTreg
CCR9
CCR5

Fig. 3

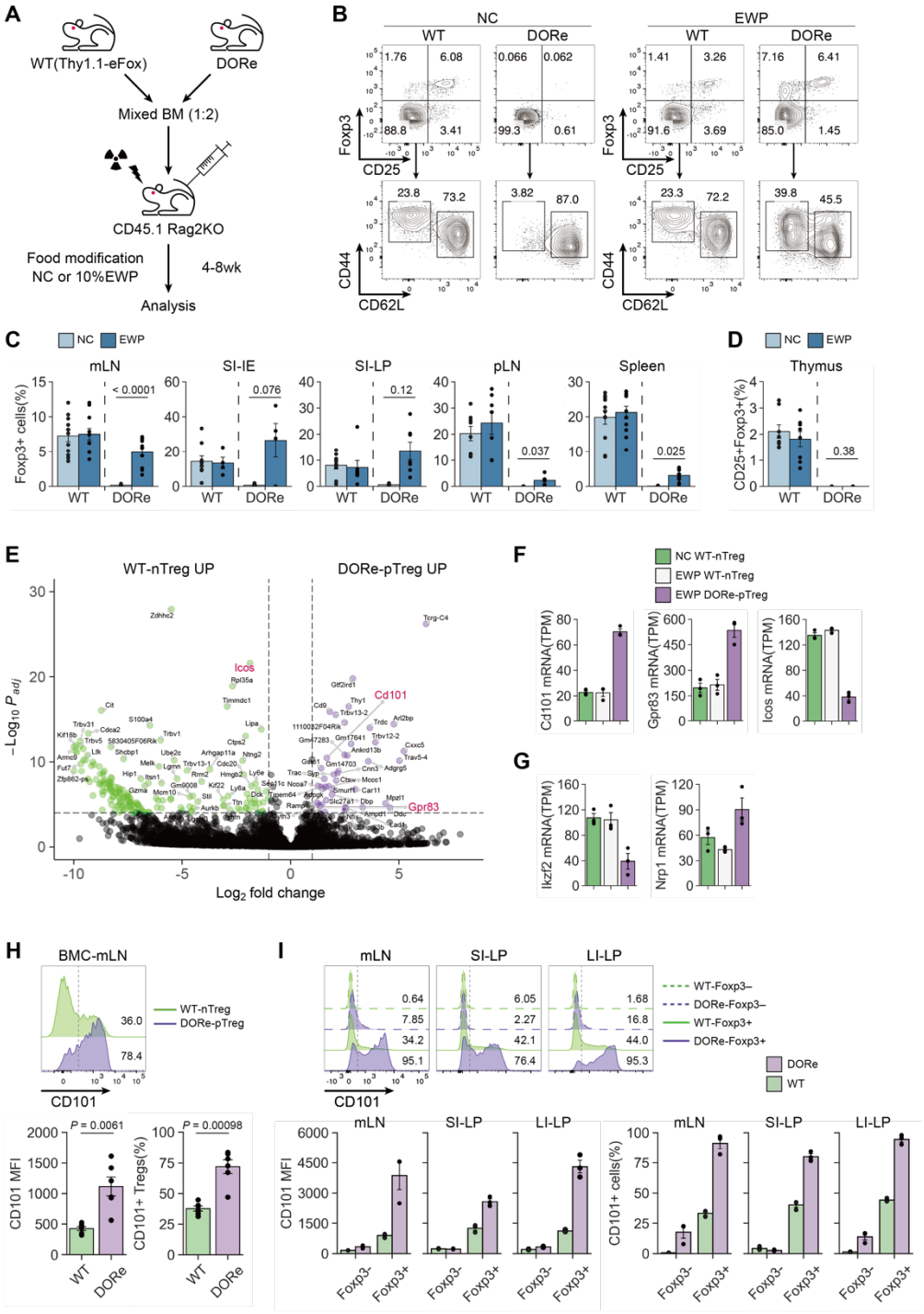
A
WT(Thy1.1-eFox)
DORe
Mixed BM (1:2)
CD45.1 Rag2KO
Food modification
NC or 10%EWP
4-8wk
Analysis
B
NC
EWP
WT
DORe
Foxp3
CD25
CD44
CD62L
C
NC
EWP
mLN
SI-IE
SI-LP
pLN
Spleen
Foxp3+ cells(%)
< 0.0001
0.076
0.12
0.037
0.025
D
Thymus
CD25+Foxp3+(%)
0.38
E
WT-nTreg UP
DORe-pTreg UP
Icos
Cd101
Gpr83
Log2 fold change
F
NC WT-nTreg
EWP WT-nTreg
EWP DORe-pTreg
Cd101 mRNA(TPM)
Gpr83 mRNA(TPM)
Icos mRNA(TPM)
G
Ikzf2 mRNA(TPM)
Nrp1 mRNA(TPM)
H
BMC-mLN
WT-nTreg
DORe-pTreg
CD101
CD101 MFI
P = 0.0061
CD101+ Tregs(%)
P = 0.00098
I
mLN
SI-LP
LI-LP
WT-Foxp3–
DORe-Foxp3–
WT-Foxp3+
DORe-Foxp3+
DORe
WT
CD101 MFI
CD101+ cells(%)
Foxp3-
Foxp3+

Fig. 4

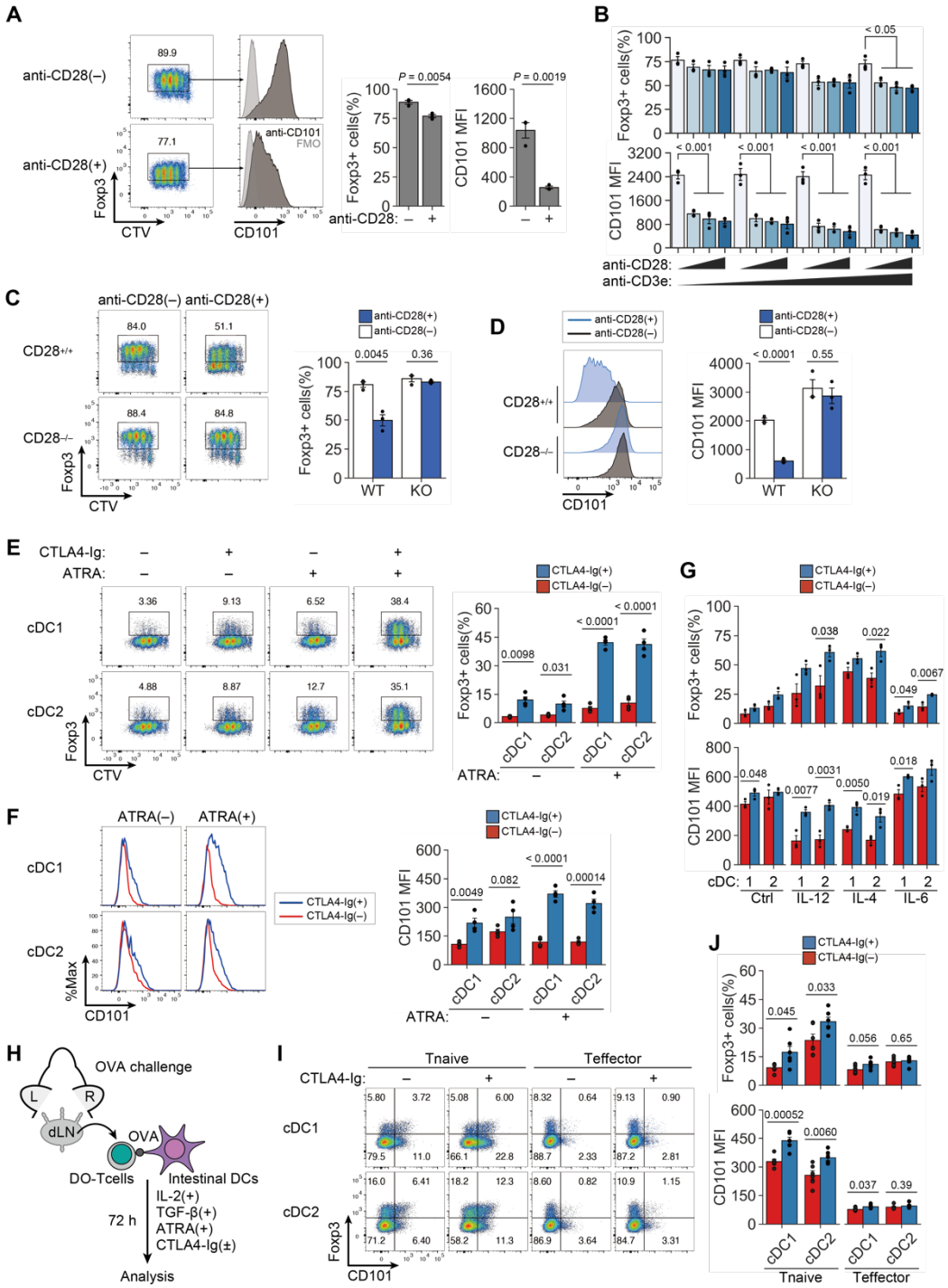
A
anti-CD28(–)
anti-CD28(+)
89.9
77.1
Foxp3
CTV
anti-CD101
FMO
CD101
P = 0.0054
P = 0.0019
Foxp3+ cells(%)
CD101 MFI
anti-CD28: – +
B
Foxp3+ cells(%)
CD101 MFI
< 0.05
< 0.001
anti-CD28:
anti-CD3e:
C
anti-CD28(–) anti-CD28(+)
CD28+/+
CD28–/–
84.0
51.1
88.4
84.8
Foxp3
CTV
anti-CD28(+)
anti-CD28(–)
0.0045
0.36
Foxp3+ cells(%)
WT
KO
D
anti-CD28(+)
anti-CD28(–)
CD28+/+
CD28–/–
CD101
< 0.0001
0.55
CD101 MFI
WT
KO
E
CTLA4-Ig:
ATRA:
cDC1
cDC2
3.36
9.13
6.52
38.4
4.88
8.87
12.7
35.1
Foxp3
CTV
CTLA4-Ig(+)
CTLA4-Ig(–)
0.0098
0.031
< 0.0001
< 0.0001
Foxp3+ cells(%)
cDC1
cDC2
ATRA: – +
G
CTLA4-Ig(+)
CTLA4-Ig(–)
0.038
0.022
0.049
0.0067
Foxp3+ cells(%)
0.048
0.0077
0.0031
0.0050
0.019
0.018
CD101 MFI
cDC: 1 2 1 2 1 2 1 2
Ctrl
IL-12
IL-4
IL-6
F
ATRA(–)
ATRA(+)
cDC1
cDC2
%Max
CD101
CTLA4-Ig(+)
CTLA4-Ig(–)
0.0049
0.082
< 0.0001
0.00014
CD101 MFI
ATRA: – +
H
OVA challenge
L
R
dLN
OVA
DO-Tcells
Intestinal DCs
72 h
IL-2(+)
TGF-β(+)
ATRA(+)
CTLA4-Ig(±)
Analysis
I
Tnaive
Teffector
CTLA4-Ig: – + – +
cDC1
cDC2
5.80
3.72
5.08
6.00
8.32
0.64
9.13
0.90
79.5
11.0
66.1
22.8
88.7
2.33
87.2
2.81
16.0
6.41
18.2
12.3
8.60
0.82
10.9
1.15
71.2
6.40
58.2
11.3
86.9
3.64
84.7
3.31
Foxp3
CD101
J
CTLA4-Ig(+)
CTLA4-Ig(–)
0.045
0.033
0.056
0.65
Foxp3+ cells(%)
0.00052
0.0060
0.037
0.39
CD101 MFI
cDC1
cDC2
cDC1
cDC2
Tnaive
Teffector

Fig. 5

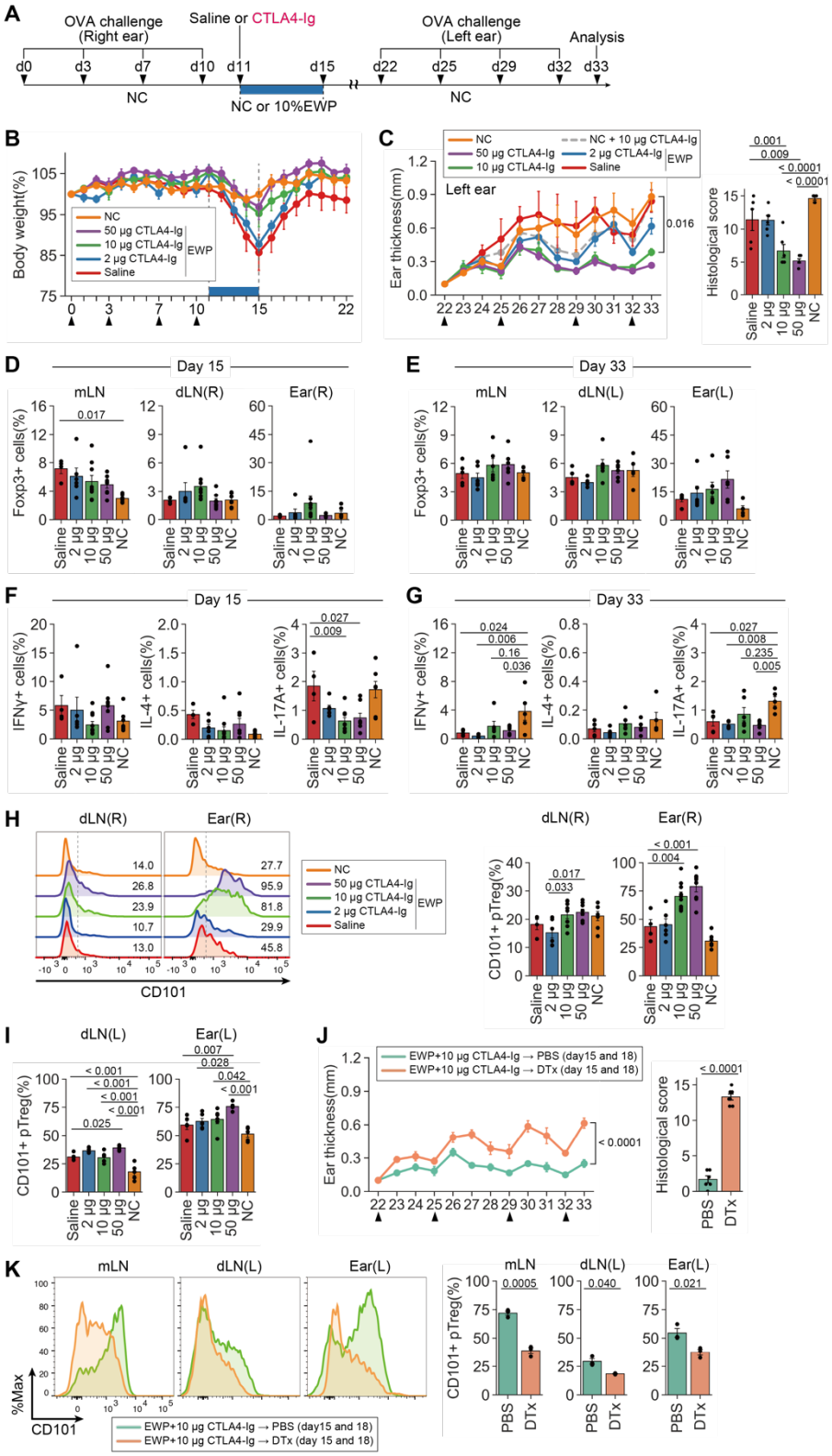
A
OVA challenge (Right ear)
Saline or CTLA4-Ig
OVA challenge (Left ear)
Analysis
d0 d3 d7 d10 d11 d15 d22 d25 d29 d32 d33
NC
NC or 10%EWP
NC
B
Body weight(%)
NC
50 μg CTLA4-Ig
10 μg CTLA4-Ig
2 μg CTLA4-Ig
Saline
EWP
C
Left ear
Ear thickness(mm)
NC + 10 μg CTLA4-Ig
Histological score
D
Day 15
mLN
dLN(R)
Ear(R)
Foxp3+ cells(%)
E
Day 33
dLN(L)
Ear(L)
F
IFNγ+ cells(%)
IL-4+ cells(%)
IL-17A+ cells(%)
G
H
CD101
CD101+ pTreg(%)
I
J
EWP+10 μg CTLA4-Ig → PBS (day15 and 18)
EWP+10 μg CTLA4-Ig → DTx (day 15 and 18)
PBS
DTx
K
%Max

Fig. 6

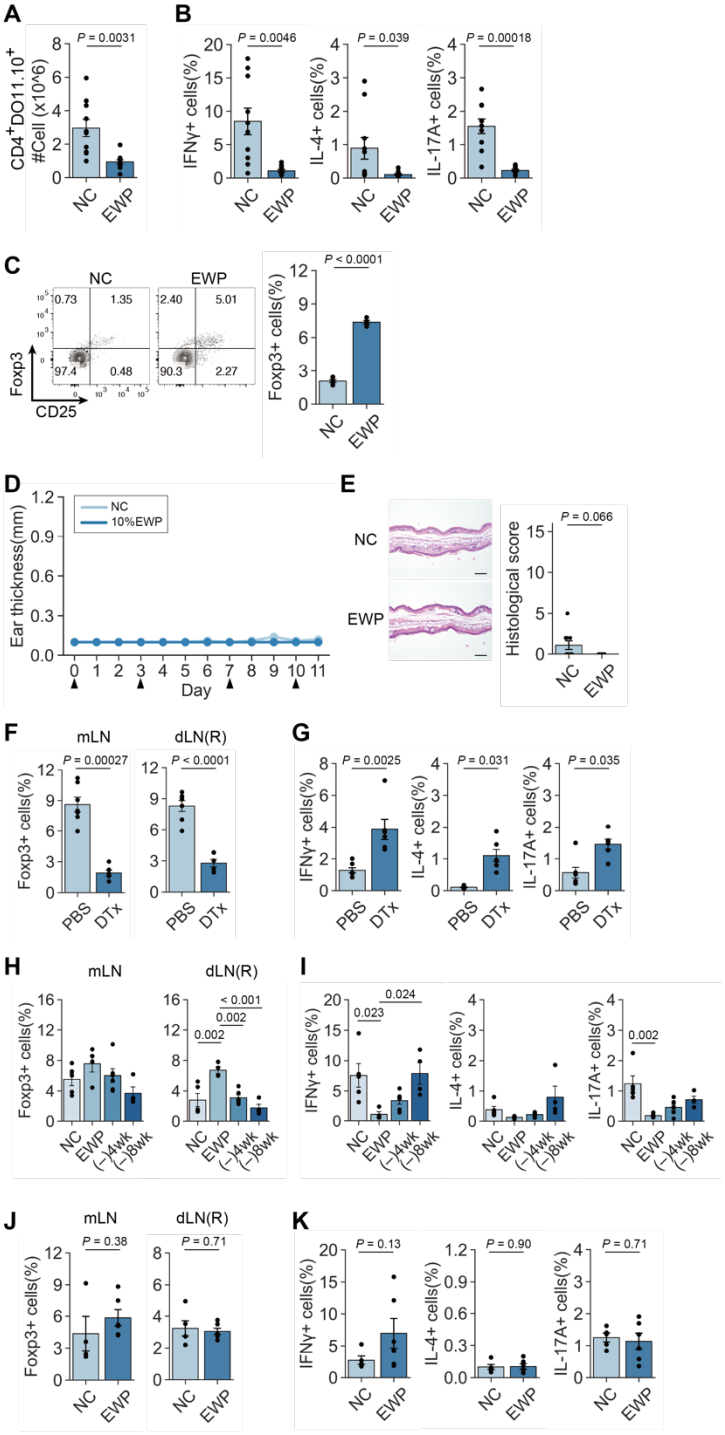
A
B
C
D
E
F
G
H
I
J
K
P = 0.0031
P = 0.0046
P = 0.039
P = 0.00018
P < 0.0001
P = 0.066
P = 0.00027
P = 0.0025
P = 0.031
P = 0.035
P = 0.38
P = 0.71
P = 0.13
P = 0.90
CD4+DO11.10+ #Cell (x10^6)
IFNγ+ cells(%)
IL-4+ cells(%)
IL-17A+ cells(%)
Foxp3+ cells(%)
Foxp3
CD25
Ear thickness(mm)
Day
Histological score
NC
EWP
10%EWP
mLN
dLN(R)
PBS
DTx
(−)4wk
(−)8wk

Fig. S1

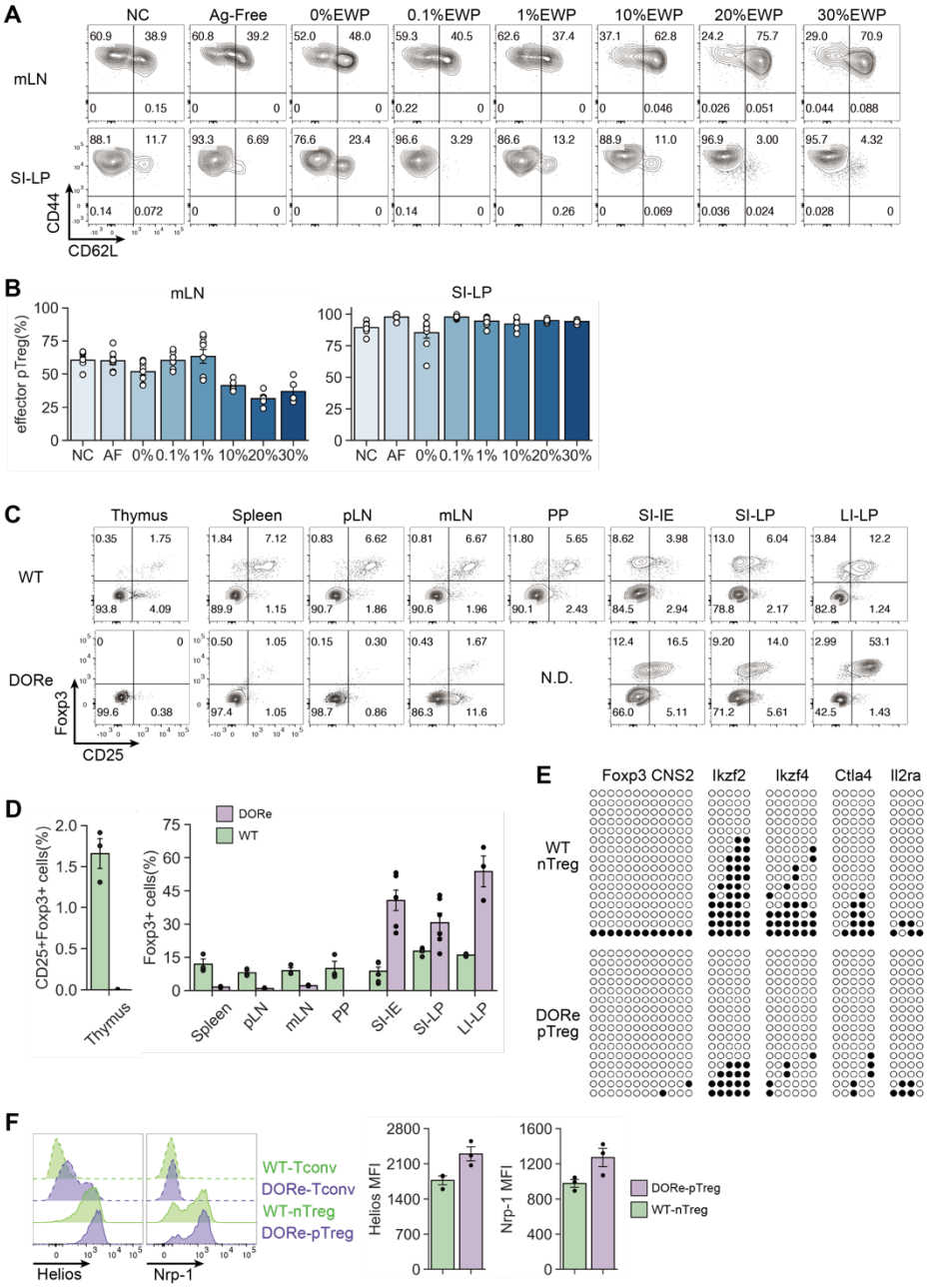
A
NC
Ag-Free
0%EWP
0.1%EWP
1%EWP
10%EWP
20%EWP
30%EWP
mLN
SI-LP
CD44
CD62L
B
mLN
SI-LP
effector pTreg(%)
NC AF 0% 0.1% 1% 10% 20% 30%
C
Thymus
Spleen
pLN
mLN
PP
SI-IE
SI-LP
LI-LP
WT
DORe
N.D.
Foxp3
CD25
D
DORe
WT
CD25+Foxp3+ cells(%)
Foxp3+ cells(%)
Thymus
Spleen
pLN
mLN
PP
SI-IE
SI-LP
LI-LP
E
Foxp3 CNS2
Ikzf2
Ikzf4
Ctla4
Il2ra
WT nTreg
DORe pTreg
F
WT-Tconv
DORe-Tconv
WT-nTreg
DORe-pTreg
Helios
Nrp-1
Helios MFI
Nrp-1 MFI
DORe-pTreg
WT-nTreg

Fig. S2

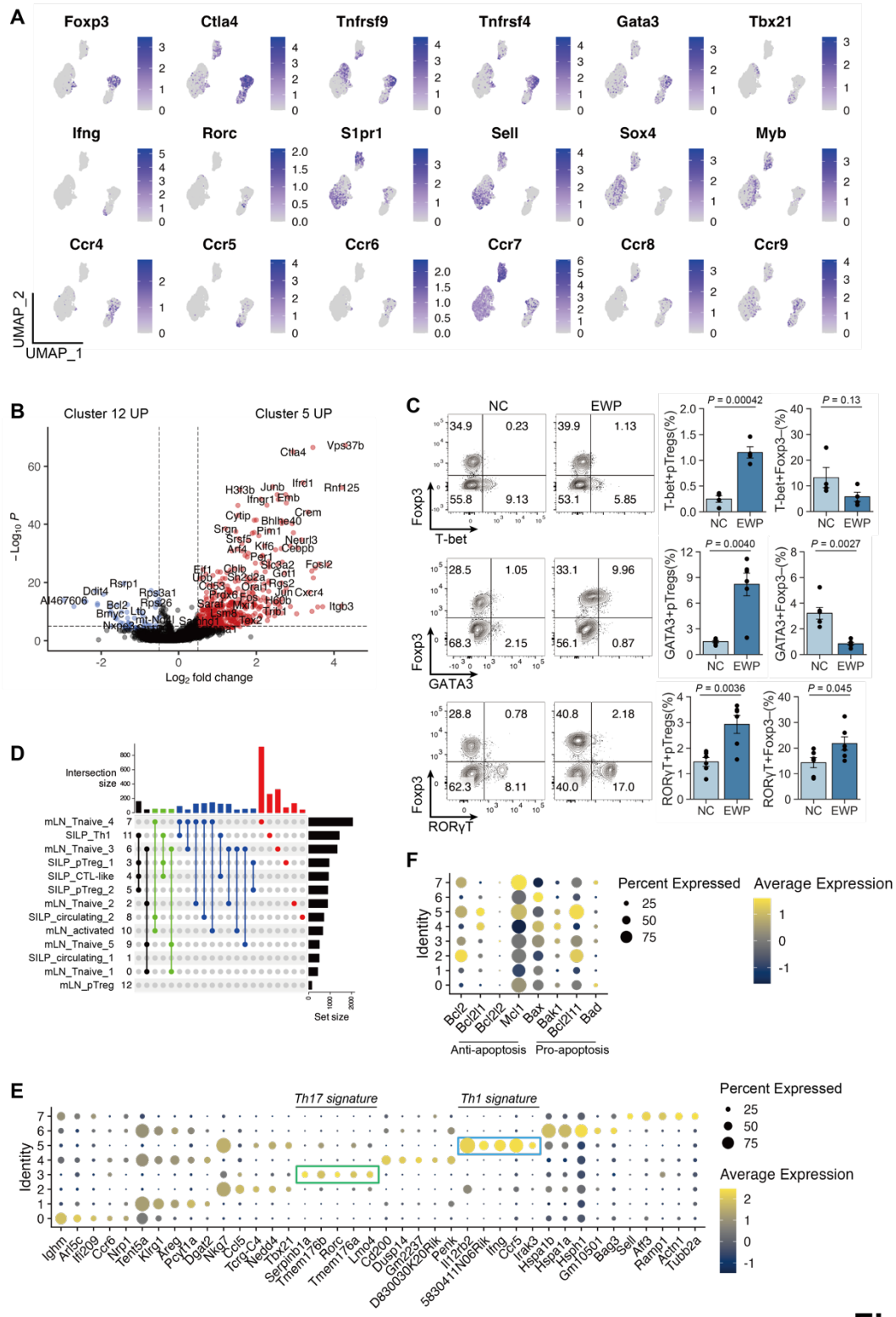
A
Foxp3
Ctla4
Tnfrsf9
Tnfrsf4
Gata3
Tbx21
Ifng
Rorc
S1pr1
Sell
Sox4
Myb
Ccr4
Ccr5
Ccr6
Ccr7
Ccr8
Ccr9
UMAP_2
UMAP_1
B
Cluster 12 UP
Cluster 5 UP
Log2 fold change
C
NC
EWP
Foxp3
T-bet
GATA3
RORγT
T-bet+pTregs(%)
T-bet+Foxp3−(%)
GATA3+pTregs(%)
GATA3+Foxp3−(%)
RORγT+pTregs(%)
RORγT+Foxp3−(%)
P = 0.00042
P = 0.13
P = 0.0040
P = 0.0027
P = 0.0036
P = 0.045
D
Intersection size
Set size
mLN_Tnaive_4
SILP_Th1
mLN_Tnaive_3
SILP_pTreg_1
SILP_CTL-like
SILP_pTreg_2
mLN_Tnaive_2
SILP_circulating_2
mLN_activated
mLN_Tnaive_5
SILP_circulating_1
mLN_Tnaive_1
mLN_pTreg
E
Th17 signature
Th1 signature
Identity
Percent Expressed
Average Expression
F
Identity
Percent Expressed
Average Expression
Anti-apoptosis
Pro-apoptosis

Fig. S3

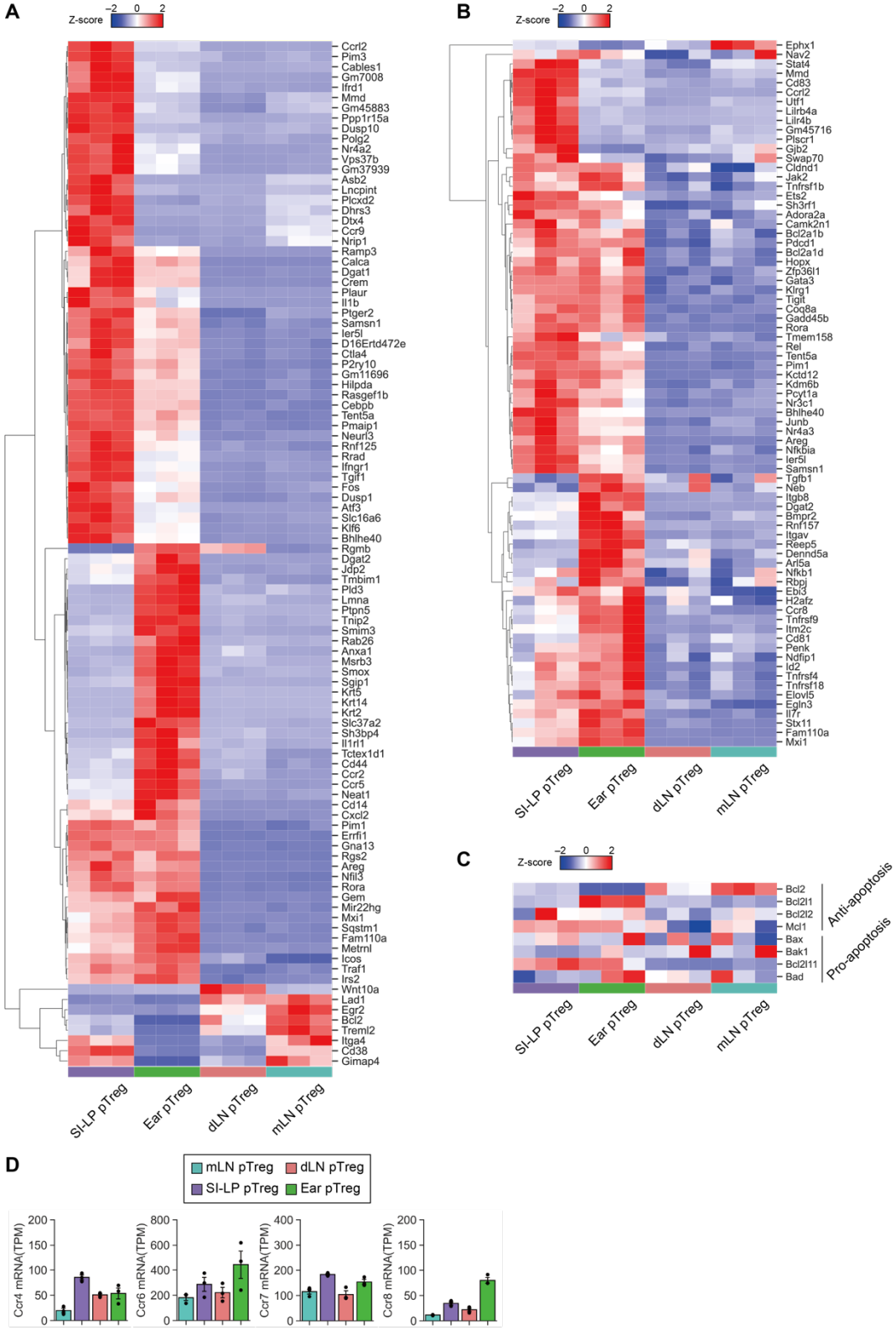
A
Z-score
−2 0 2
Ccrl2
Pim3
Cables1
Gm7008
Ifrd1
Mmd
Gm45883
Ppp1r15a
Dusp10
Polg2
Nr4a2
Vps37b
Gm37939
Asb2
Lncpint
Plcxd2
Dhrs3
Dtx4
Ccr9
Nrip1
Ramp3
Calca
Dgat1
Crem
Plaur
Il1b
Ptger2
Samsn1
Ier5l
D16Ertd472e
Ctla4
P2ry10
Gm11696
Hilpda
Rasgef1b
Cebpb
Tent5a
Pmaip1
Neurl3
Rnf125
Rrad
Ifngr1
Tgif1
Fos
Dusp1
Atf3
Slc16a6
Klf6
Bhlhe40
Rgmb
Dgat2
Jdp2
Tmbim1
Pld3
Lmna
Ptpn5
Tnip2
Smim3
Rab26
Anxa1
Msrb3
Smox
Sgip1
Krt5
Krt14
Krt2
Slc37a2
Sh3bp4
Il1rl1
Tctex1d1
Cd44
Ccr2
Ccr5
Neat1
Cd14
Cxcl2
Pim1
Errfi1
Gna13
Rgs2
Areg
Nfil3
Rora
Gem
Mir22hg
Mxi1
Sqstm1
Fam110a
Metrnl
Icos
Traf1
Irs2
Wnt10a
Lad1
Egr2
Bcl2
Treml2
Itga4
Cd38
Gimap4
Sl-LP pTreg
Ear pTreg
dLN pTreg
mLN pTreg
B
Z-score
−2 0 2
Ephx1
Nav2
Stat4
Mmd
Cd83
Ccrl2
Utf1
Lilrb4a
Lilr4b
Gm45716
Plscr1
Gjb2
Swap70
Cldnd1
Jak2
Tnfrsf1b
Ets2
Sh3rf1
Adora2a
Camk2n1
Bcl2a1b
Pdcd1
Bcl2a1d
Hopx
Zfp36l1
Gata3
Klrg1
Tigit
Coq8a
Gadd45b
Rora
Tmem158
Rel
Tent5a
Pim1
Kctd12
Kdm6b
Pcyt1a
Nr3c1
Bhlhe40
Junb
Nr4a3
Areg
Nfkbia
Ier5l
Samsn1
Tgfb1
Neb
Itgb8
Dgat2
Bmpr2
Rnf157
Itgav
Reep5
Dennd5a
Arl5a
Nfkb1
Rbpj
Ebi3
H2afz
Ccr8
Tnfrsf9
Itm2c
Cd81
Penk
Ndfip1
Id2
Tnfrsf4
Tnfrsf18
Elovl5
Egln3
Il7r
Stx11
Fam110a
Mxi1
Sl-LP pTreg
Ear pTreg
dLN pTreg
mLN pTreg
C
Z-score
−2 0 2
Bcl2
Bcl2l1
Bcl2l2
Mcl1
Bax
Bak1
Bcl2l11
Bad
Anti-apoptosis
Pro-apoptosis
Sl-LP pTreg
Ear pTreg
dLN pTreg
mLN pTreg
D
mLN pTreg
dLN pTreg
Sl-LP pTreg
Ear pTreg
Ccr4 mRNA(TPM)
Ccr6 mRNA(TPM)
Ccr7 mRNA(TPM)
Ccr8 mRNA(TPM)

Fig. S4

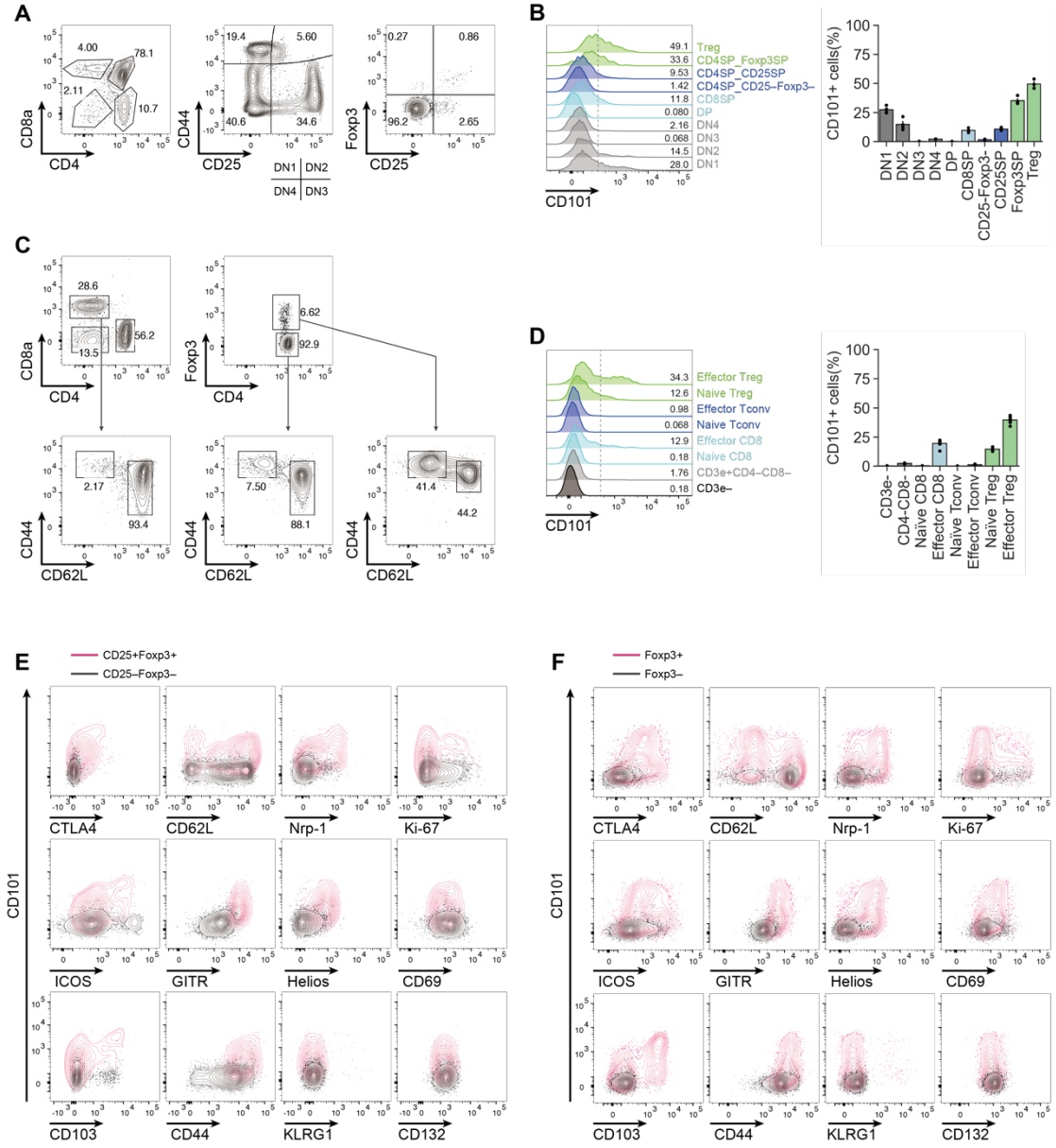
A
CD8a
CD4
4.00
78.1
2.11
10.7
CD44
CD25
19.4
5.60
40.6
34.6
DN1
DN2
DN4
DN3
Foxp3
CD25
0.27
0.86
96.2
2.65
B
CD101
49.1 Treg
33.6 CD4SP_Foxp3SP
9.53 CD4SP_CD25SP
1.42 CD4SP_CD25–Foxp3–
11.8 CD8SP
0.080 DP
2.16 DN4
0.068 DN3
14.5 DN2
28.0 DN1
CD101+ cells(%)
100
75
50
25
0
DN1
DN2
DN3
DN4
DP
CD8SP
CD25-Foxp3-
CD25SP
Foxp3SP
Treg
C
CD8a
CD4
28.6
56.2
13.5
Foxp3
CD4
6.62
92.9
CD44
CD62L
2.17
93.4
7.50
88.1
41.4
44.2
D
CD101
34.3 Effector Treg
12.6 Naive Treg
0.98 Effector Tconv
0.068 Naive Tconv
12.9 Effector CD8
0.18 Naive CD8
1.76 CD3e+CD4–CD8–
0.18 CD3e–
CD101+ cells(%)
100
75
50
25
0
CD3e-
CD4-CD8-
Naive CD8
Effector CD8
Naive Tconv
Effector Tconv
Naive Treg
Effector Treg
E
CD25+Foxp3+
CD25–Foxp3–
CD101
CTLA4
CD62L
Nrp-1
Ki-67
ICOS
GITR
Helios
CD69
CD103
CD44
KLRG1
CD132
F
Foxp3+
Foxp3–
CD101
CTLA4
CD62L
Nrp-1
Ki-67
ICOS
GITR
Helios
CD69
CD103
CD44
KLRG1
CD132

Fig. S5

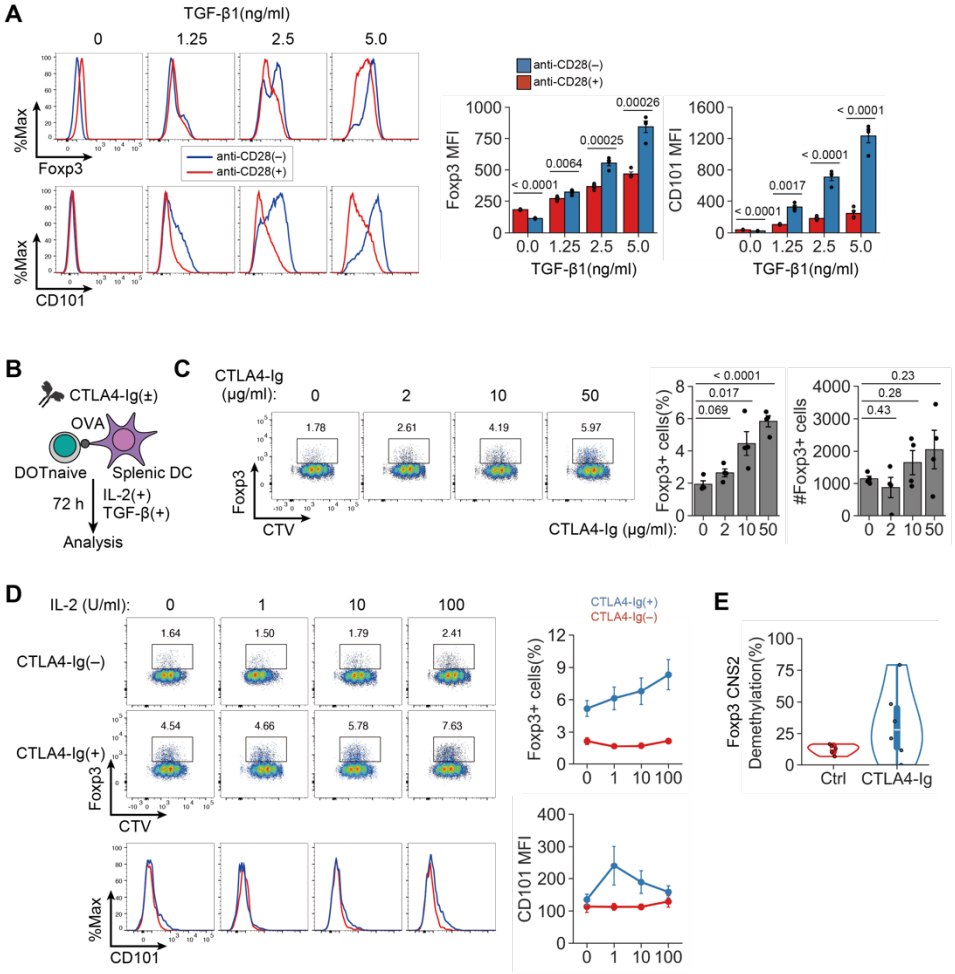
A
TGF-β1(ng/ml)
0
1.25
2.5
5.0
%Max
Foxp3
CD101
anti-CD28(–)
anti-CD28(+)
Foxp3 MFI
CD101 MFI
TGF-β1(ng/ml)
< 0.0001
0.0064
0.00025
0.00026
0.0017
B
CTLA4-Ig(±)
OVA
DOTnaive
Splenic DC
72 h
IL-2(+)
TGF-β(+)
Analysis
C
CTLA4-Ig
(μg/ml):
1.78
2.61
4.19
5.97
CTV
Foxp3+ cells(%)
#Foxp3+ cells
0.017
0.069
0.23
0.28
0.43
D
IL-2 (U/ml):
CTLA4-Ig(–)
CTLA4-Ig(+)
1.64
1.50
1.79
2.41
4.54
4.66
5.78
7.63
CTLA4-Ig(+)
CTLA4-Ig(–)
E
Foxp3 CNS2
Demethylation(%)
Ctrl
CTLA4-Ig

Fig. S6

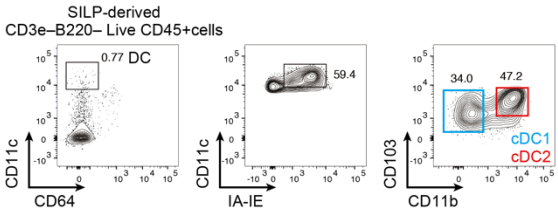
SILP-derived
CD3e–B220– Live CD45+cells
0.77 DC
CD11c
CD64
59.4
CD11c
IA-IE
34.0
47.2
cDC1
cDC2
CD103
CD11b

Fig. S7

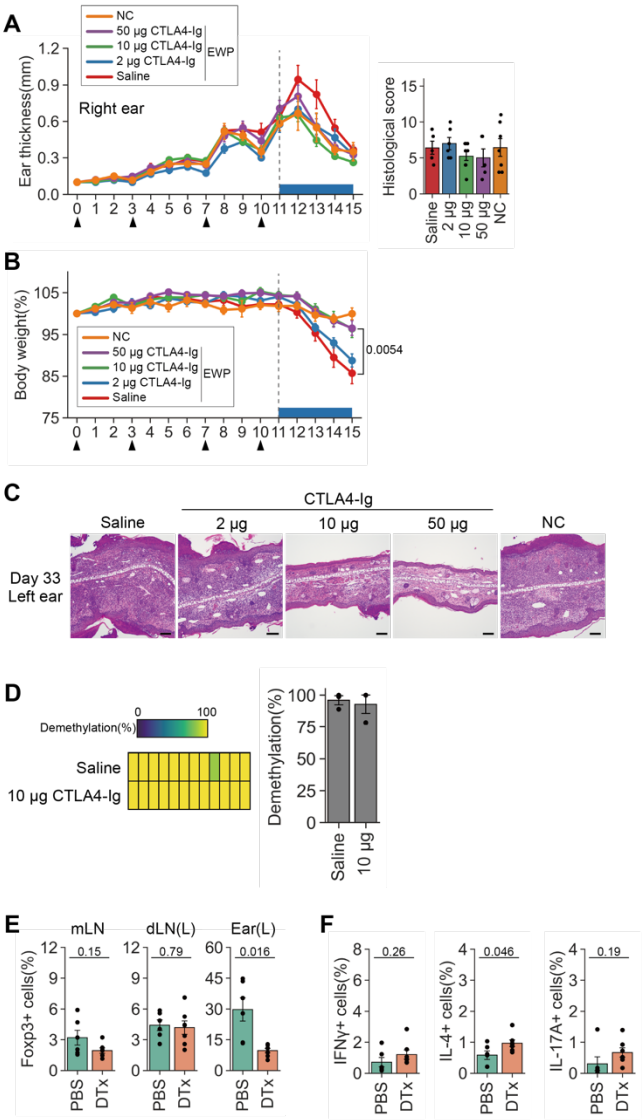
A
NC
50 μg CTLA4-Ig
10 μg CTLA4-Ig
2 μg CTLA4-Ig
Saline
EWP
Right ear
Ear thickness(mm)
Histological score
Saline
2 μg
10 μg
50 μg
NC
B
Body weight(%)
0.0054
C
CTLA4-Ig
Saline
2 μg
10 μg
50 μg
NC
Day 33
Left ear
D
Demethylation(%)
Saline
10 μg CTLA4-Ig
E
mLN
dLN(L)
Ear(L)
Foxp3+ cells(%)
0.15
0.79
0.016
PBS
DTx
F
IFNγ+ cells(%)
0.26
IL-4+ cells(%)
0.046
IL-17A+ cells(%)
0.19

Fig. S8

Table S1. Nutrition facts of modified food

CE-2 (Normal Chow; NC)

Nutrition facts	(%)
Water	8.84
Crude protein	25.48
Crude fat	4.61
Crude fiber	5.14
Crude ash	7.01
Nitrogen free extract	48.92
Total	100.00

CE-2 (–)White fish powder (0%EWP)

Nutrition facts	(%)
Water	9.00
Crude protein	19.86
Crude fat	4.26
Crude fiber	5.30
Crude ash	6.24
Nitrogen free extract	55.34
Total	100.00

Modified food

ID	CE-2 (–)White fish powder (%)	Corn starch (%)	EWP (%)	EWP derived protein (%)
0%EWP	100	0	0	0
0.1%EWP	99.89961	0.07743	0.02296	0.10000
1%EWP	98.99610	0.77431	0.22959	1.00000
10%EWP	89.96105	7.74300	2.29595	10.00000
20%EWP	79.92200	15.48609	4.59191	20.00000
30%EWP	69.88305	23.22909	6.88786	30.00000

Table S2. List of antibodies

Antibodies used for flowcytometry, FACS sorting, and other experiments

Antibodies	Manufacturer	Identifier
Anti-mouse CD3e-APC (145-2C11)	BD pharmingen	Cat#553066; RRID: AB_398529
Anti-mouse CD3e-APC-Cy7 (145-2C11)	BioLegend	Cat#100330; RRID: AB_1877170
Anti-mouse CD3e-Biotin (145-2C11)	BD Biosciences	Cat#553060; RRID: AB_394593
Anti-mouse CD3e-PE (145-2C11)	Invitrogen	Cat#12-0031-82; RRID: AB_465496
Anti-mouse CD3e-V500 (500A2)	BD Biosciences	Cat#560771; RRID: AB_1937314
Anti-mouse CD4-AF700 (RM4-5)	Invitrogen	Cat#56-0042-82; RRID: AB_494000
Anti-mouse CD4-V500 (RM4-5)	BD Biosciences	Cat#560782; RRID: AB_1937327
Anti-mouse CD4-BV650 (RM4-5)	BD Biosciences	Cat#563747; RRID: AB_2716859
Anti-mouse CD8a-PerCP-Cy5.5 (53-6.7)	BD Biosciences	Cat#551162; RRID: AB_394081
Anti-mouse CD11b-AF700 (M1/70)	Invitrogen	Cat#56-0112-80; RRID: AB_657585
Anti-mouse CD11b-PerCP-Cy5.5 (M1/70)	Invitrogen	Cat#45-0112-82; RRID: AB_468714
Anti-mouse CD11c-BV605 (N418)	BIoLegend	Cat#117334; RRID: AB_2562415
Anti-mouse CD11c-PE-Cy7 (N418)	BioLegend	Cat#117318; RRID: AB_493568
Purified anti-mouse CD16/32 (93)	BioLegend	Cat#101302; RRID: AB_312801
Anti-mouse CD25-BV421 (PC61)	BioLegend	Cat#102034; RRID: AB_11203373
Anti-mouse CD25-PE (PC61)	BD pharmingen	Cat#553866; RRID: AB_395101
Anti-mouse CD25-PE-Cy7 (PC61)	BD Biosciences	Cat#552880; RRID: AB_394509
Anti-mouse CD25-PerCP-Cy5.5 (PC61)	BD Biosciences	Cat#551071; RRID: AB_394031
Anti-mouse CD44-APC (IM7)	Invitrogen	Cat#17-0441-83; RRID: AB_469390
Anti-mouse CD44-PE-Cy7 (IM7)	Invitrogen	Cat#25-0441-82; RRID: AB_469623
Anti-mouse CD44-V500 (IM7)	BD Biosciences	Cat#560780; RRID: AB_1937328
Anti-mouse CD45-BV510 (30-F11)	BioLegend	Cat#103138; RRID: AB_2563061
Anti-mouse CD45.1-APC-Cy7 (A20)	BioLegend	Cat#110716; RRID: AB_313505
Anti-mouse/human CD45R/B220-APC-eFluor780 (RA3-6B2)	Invitrogen	Cat#47-0452-82; RRID: AB_1518810
Anti-mouse/human CD45R/B220-Biotin (RA3-6B2)	BioLegend	Cat#103204; RRID: AB_312989
Anti-mouse CD62L-BV421 (MEL-14)	BD Biosciences	Cat#562910; RRID: AB_2737885
Anti-mouse CD62L-PerCP-Cy5.5 (MEL-14)	BD pharmingen	Cat#560513; RRID: AB_10611578
Anti-mouse CD64-PE (X54-5/7.1)	BioLegend	Cat#139304; RRID: AB_10612740
Anti-mouse CD90.1-BV605 (OX-7)	BD Biosciences	Cat#740374; RRID: AB_2740106
Anti-mouse CD90.1-PerCP (OX-7)	BD Biosciences	Cat#557266; RRID: AB_396611
Anti-mouse CD90.2-AF700 (53-2.1)	BioLegend	Cat#140324; RRID: AB_2566740
Anti-mouse CD90.2-PE-Cy7 (53-2.1)	BioLegend	Cat#140310; RRID: AB_10643586
Anti-mouse CD101-APC (REA301)	Miltenyi Biotec	Cat#130-104-304; RRID: AB_2654344
Anti-mouse CD101-PE (REA301)	Miltenyi Biotec	Cat#130-120-173; RRID: AB_2752032
Anti-mouse CD101-PE-Vio770 (REA301)	Miltenyi Biotec	Cat#130-104-305; RRID: AB_2654345
Anti-mouse CD103-APC (2E7)	Invitrogen	Cat#17-1031-82; RRID: AB_1106992

Anti-mouse CD103-PE-Cy7 (2E7)	BioLegend	Cat#121426; RRID: AB_2563691
Anti-mouse CD134(OX40)-BV421 (OX-86)	BioLegend	Cat#119411; RRID: AB_10962569
Anti-mouse CD134(OX40)-PE (OX-86)	BioLegend	Cat#119410; RRID: AB_2207344
Anti-mouse CD137(4-1BB)-APC (17B5)	BioLegend	Cat#106110; RRID: AB_2564297
Anti-mouse CD195(CCR5)-BV421 (C34-3448)	BD Biosciences	Cat#743695; RRID: AB_2741677
Anti-mouse CD199(CCR9)-PE (CW-1.2)	BioLegend	Cat#128710; RRID: AB_1227479
Anti-mouse CD278(ICOS)-PE-Cy7 (C398.4A)	BioLegend	Cat#313520; RRID: AB_10643411
Anti-mouse CD304(Neuropilin-1)-eFluor450 (3DS304M)	Invitrogen	Cat#48-3041-82; RRID: AB_2574051
Anti-mouse CD304(Neuropilin-1)-PE-Cy7 (3DS304M)	Invitrogen	Cat#25-3041-82; RRID: AB_2573436
Anti-mouse CD357(GITR)-PE-Cy7 (DTA-1)	BD Biosciences	Cat#558140; RRID: AB_647252
Anti-mouse/human Helios-APC (22F6)	BioLegend	Cat#137218; RRID: AB_10660750
Anti-mouse/human Helios-PE-Cy7 (22F6)	BioLegend	Cat#137236; RRID: AB_2565990
Anti-mouse I-A/I-E-BV421 (M5/114.15.2)	BioLegend	Cat#107631; RRID: AB_10900075
Anti-mouse I-A/I-E-BV510 (M5/114.15.2)	BioLegend	Cat#107635; RRID: AB_2561397
Anti-mouse/human Ki-67-PE-Cy7 (SolA15)	Invitrogen	Cat#25-5698-82; RRID: AB_11220070
Anti-mouse/human KLRG1-PerCP-Cy5.5 (2F1/KLRG1)	BioLegend	Cat#138418; RRID: AB_2563014
Anti-mouse/human T-bet-BV421 (4B10)	BioLegend	Cat#644816; RRID: AB_2686976
Anti-mouse TCR DO11.10-APC (KJ1-26)	Invitrogen	Cat#17-5808-80; RRID: AB_469459
Anti-mouse TCR DO11.10-PerCP-Cy5.5 (KJ1-26)	BioLegend	Cat#118512; RRID: AB_2028522
Anti-mouse TER-119/Erythroid Cells-Biotin (TER-119)	BD pharmingen	Cat#553672; RRID: AB_394985
Anti-mouse TIGIT-APC (1G9)	BioLegend	Cat#142105; RRID: AB_10960139
Anti-mouse Foxp3-Alexa Fluor 488 (FJK-16s)	Invitrogen	Cat#53-5773-82; RRID: AB_763537
Anti-human/mouse Gata3-eFlour660 (TWAJ)	Invitrogen	Cat#50-9966-42; RRID: AB_10596663
Anti-mouse RORgamma(t)-PE (B2D)	Invitrogen	Cat#12-6981-82; RRID: AB_10807092
Anti-mouse IL-4-APC (11B11)	Invitrogen	Cat#17-7041-82; RRID: AB_469494
Anti-mouse IL-17A-BV421 (TC11-18H10.1)	BioLegend	Cat#506925; RRID: AB_10900442
Anti-mouse IFN gamma-PE (XMG1.2)	Invitrogen	Cat#12-7311-82; RRID: AB_466193
TotalSeq-C0301 anti-mouse Hashtag 1 Antibody	BioLegend	Cat#155861; RRID: AB_2800693
TotalSeq-C0302 anti-mouse Hashtag 2 Antibody	BioLegend	Cat#155863; RRID: AB_2800694
TotalSeq-C0303 anti-mouse Hashtag 3 Antibody	BioLegend	Cat#155865; RRID: AB_2800695
TotalSeq-C0304 anti-mouse Hashtag 4 Antibody	BioLegend	Cat#155867; RRID: AB_2800696
Purified NA/LE anti-mouse CD3e (145-2C11)	BD pharmingen	Cat#553057; RRID: AB_394590
Purified NA/LE anti-mouse CD28 (37.51)	BD pharmingen	Cat#553294; RRID: AB_394763
Anti-Histone H3 Acetyl Lys27	GeneTex	Cat#GTX60815; RRID: AB_2888004